Preprints are preliminary reports that have not undergone peer review.
They should not be considered conclusive, used to inform clinical practice,
or referenced by the media as validated information.

Modeling of above-ground biomass of pure Calabrian pine (Pinus brutia Ten.) stands using Sentinel-2 time series and Sentinel-1 imagery; a case study from the south of Turkey

Hasan AKSOY (haksoy@sinop.edu.tr)
Sinop University, Program of Forestry and Forest Products

Research Article

Keywords: Above-ground biomass, Sentinel, Topography, Multiple linear regression

Posted Date: May 17th, 2023

DOI: https://doi.org/10.21203/rs.3.rs-2902455/v1

License: This work is licensed under a Creative Commons Attribution 4.0 International License. Read Full License

Abstract

Aboveground biomass (AGB) is an important source of information for natural resource conservation at spatial scales, accurate determination of carbon stocks and climate containment systems, and sustainable resource conservation planners. This study, it was aimed to model the Above-ground biomass (AGB) of pure Calabrian pine (*Pinus brutia* Ten.) stands in southern Turkey. In the study, digital band, reflectance, and vegetation indices values obtained from Sentinel-2 satellite images of rainy, semi-arid and dry seasons were used to measure the effect of seasonality on the modeling of the AGB. Digital band, reflectance (VV/VH polarization), and backscatter values were also used from the Sentinel-1 satellite image. In addition to all these, topographic data of the study area was used as an independent variable. The multiple linear regression (MLR) method was used in the modeling of AGB and the most successful model was tried to be determined by the relative rank method. A total of 33 models were obtained by creating data sets with the independent variables first one by one and then with each other in combination. The highest model success of AGB was obtained in the data set created by the integration of digital band and vegetation indices, Sentinel-1 (S1) reflectance, and topographic values of Sentinel-2 (S2) images taken in rainy and semi-arid seasons (R^2=0.49; RMSE=26.21 ton ha^{-1}; MAE=22.50 ton ha^{-1}; BIC=5.42; AIC= 21.23; R_j=57.68). It was observed that the integration of topographic data into each dataset increased the modeling success in all models. In addition, it was observed that the highest success in modeling the AGB with the data obtained from Sentinel-2 was obtained in the rainy season data. In particular, it was seen that the combination of S2, S1, and topographic data would contribute to the prediction accuracy of AGB.

1. Introduction

In terrestrial ecosystems, forest ecosystems have a very important role in regulating carbon emissions, water and energy cycles and global climate (Herold et al., 2019; Puliti et al., 2021). Determining the above-ground biomass (AGB) of forests is important in terms of revealing the impact of sustainable forest management on climate change (Eggleston et al., 2006; Duncanson et al., 2021). The detection of AGB in forests provides valuable information for forestry strategic planning (Gallaun et al., 2010), sheds light on the monitoring of ecosystem productivity (Finegan et al., 2015), forest fires (Di Giuseppe et al., 2021), and changes in forests over time (Puliti et al., 2021). AGB can be determined by field measurements (Brown and Iverson. 1992; Schroeder et al., 1997; Brown, 2002) and remote sensing (RS) methods (Tiwari, 1994; Roy and Ravan, 1996; Nelson et al., 2000; Tomppo et al., 2002; Foody et al., 2003; Zheng et al., 2004; Lu, 2005; Güverçin and Günlü, 2023). Determination of forest AGB by traditional field measurement methods provideshigh-accuracyy results. However, these processes have some disadvantages such as taking a lot of time, being costly, and requiring labor for tree cutting (Bulut, 2023). The remote sensing method is often preferred to eliminate the important disadvantages of field measurements and to make AGB estimates with high accuracy (Fararoda et al., 2021; Liu and Popescu, 2022; López-Serrano et al., 2019; Turgut and Günlü, 2022; Bulut, 2023). Landsat (Dogru et al., 2020), Worldview-2 (Zhu et al., 2015), QuickBird (Macedo et al., 2018), radar (Soja et al., 2021) and light detection and range determination (LiDAR) (Salum et al., 2021; Bulut, 2023) are widely used satellite images, especially in terms of optical sensors, which have medium spatial resolution and are freely accessible. Landsat and Sentinel satellite images are the most frequently used satellites because they are freely available in the estimation of the AGB. Studies in which AGB was estimated with data obtained from Landsat 8 OLI and Sentinel-2 satellite imagery showed that these satellites have spatial and spectral capabilities in estimating AGB (Sibanta et al., 2016; Forkuor et al., 2018). It has been stated that active sensors such as Sentinel-1 and ALOS-PALSAR can be used in the estimation of AGB and in determining vegetation information with backscatter values (Lucas et al., 2008; Berninger et al., 2019). The fact that active satellites (such as Sentinel-1) can collect data and pass through forest cover in all weather conditions both day and night makes them more advantageous compared to optical satellites (Santos et al., 2002; David et al., 2022). Recently, there are many many studies using forest areas. For example; Powell et al. (2010) and Main-Knorn et al. (2013) tried to model and map the AGB with Landsat images. Open access high rhigh-resolutional (Sentinel-2) (Drusch et al., 2012) and SAR (Sentinel-1) Torres et al., (2012) satellite images provided by Copernicus have also started to be used in terrestrial research applications and AGB estimation. Chen et al., (2018) modeled AGB with the data obtained from Sentinel-1 and Sentinel-2 satellite images, both individually and with the combination of the data. In another study, the AGB was tried to be estimated using a Sentinel-1 satellite image (Laurin et al., 2018; Li et al., 2020; Puliti 2021). To increase the model success of AGB, it is possible to come across studies in which remote sensing data and topographic data are integrated (Liu et al., 2019; Hu et al., 2020). In AGB modeling, many methods such as multiple linear regression, machine learning, artificial neural networks, support vector machines, and random forest algorithms are used (Forkuor et al., 2020). Multiple linear regression is the most commonly used method for modeling the linear relationship between AGB and independent variables (Turgut and Günlü, 2022).

This study was carried out in pure Calabrian pine (*Pinus brutia Ten.*) stands, which are naturally distributed in the South of Turkey (Mediterranean region). Multiple linear regression of pure Calabrian pine stands AGB using digital band, reflectance, and vegetation indices obtained from Sentinel-2 time series (rainy-semi-arid and dry), digital band, reflectance, and backscatter obtained from Sentinel-1 satellite image, and topographic data It was aimed to model using the method. In addition, in the study, it was aimed to determine the modeling ability of AGB, the effects of including topographic data in the modeling, and the effects of seasonality in the modeling of AGB by creating data sets obtained from Sentinel-2 and Sentinel-1 satellite images individually or in combination.

2. Material and Method

2.1.Material

2.1.1. Study Area and Data

The study was carried out in pure Calabrian pine fields of the Antalya Regional Directorate of Forestry, Serik Forestry Management Directorate, Akbas, and Serik Forestry Operations Chiefdom. The working boundary is located between 30^0 .87' – 31^0.32' north latitude and 37^0 .23' – 36^0.81' east longitude. The study area covers an area of 124,227.00 ha. 51% (63,075.00 ha) of the area is forested and 49% (61,152.00 ha) is non-forest. 72% of the forest area is 45,675.5 ha normal grove and 28% is 17,399.00 ha degraded grove forest. The average land height of the study area is 151.42 m. The dominant tree species of the area is Calabrian pine (Anon., 2021). The map showing the geographical location of the study area is shown in Fig. 1.

In the study, forest management inventories s of the diameter data at breast height ($d_{1.3}$) of trees 8 cm and above in 224 sample plots, which were systematically determined at 300 x 300m spacing distance for pure Calabrian pine stands, were used. Sentinel-2 satellite image for 26.05.2021–24.08.2021 and 22.11.2021, Sentinel-1A satellite image dated 26.11.2021, and ALOS-PALSAR image for digital elevation model, regarding the year of the measurements were obtained. The properties of Sentinel-2 and Sentinel-1A satellite images are shown in Table 1 and Table 2 (Nasa 2021).

Table 1
Technical specifications of Sentinel-2 satellite image

Bant	Electromagnetic Field	Wavelength (nm)	Spatial Resolution (m)
S2	Blue	458–523	10
S3	Green	543–578	10
S4	red	650–680	10
S5	Red Edge 1	698–713	20
S6	Red Edge 2	733–748	20
S7	NIRNarrow 1	773–793	20
S8	NIR	785–900	10
S8A	NIRNarrow 2	855–875	20
S11	SWIR 1	1565–1655	20
S12	SWIR 2	2100–2280	20

Table 2
Technical specifications of Sentinel-1A satellite image

Sentinel-1	Specifications
Launch Dates	S1-A, 3 April 2014 - S1-B, 25 April 2016
Launch Site and Vehicle	French Guina, Soyuz rocket
Data Capacity	1410gb
Satellite Weight	2300 kg
Orbital Elevation	693 km
Orbit Type	Sun-synchronous, near-polar, circular orbit
Sensor	C-SAR (C-bant Synthetic Aperture Radar)
Temporal Resolution	12 days

2.2.Method

In the study, the Above Ground Biomass (AGB) of each sample plot was calculated using the $d_{1.3}$ diameters of the trees in each sample plot. Then, digital band, reflectance, and vegetation indices from Sentinel-2 satellite images of three different dates, digital band, backscatter, and polarization from Sentinel-1A satellite images, and finally elevation, aspect, and slope data from ALOS-PALSAR images were calculated. The diagram showing the general workflow of the study is shown in Fig. 2.

2.2.1. Calculation of Above-Ground Biomass Values for Sample Plots

Diameter data for each sample area were obtained from the inventory scorecards of pure Calabrine pine stands obtained from the Forestry Administration and Planning Department. Then, by using the $d_{1.3}$ diameter of each tree in the sample plot, the AGB of a single tree was calculated, and the total AGB of the sample area was calculated by summing the AGB of the trees in the sample plot. Finally, the total AGB per hectare was calculated by multiplying the AGB for each sample area (400, 600, and 800 m^2) with the conversion factor to hectare. In the calculation of above-ground biomass, the single-entry above-ground biomass equation developed by Şahin (2015) for pure Calabrian pine stands distributed within the boundaries of Mersin Regional Directorate of Forestry was used (Equ. 1) (R^2 = 0.957, S_{yx}=88.988).

$$\ln\left(AGB\right) = -2.80486 + \frac{2.16137}{d} + 2.41102ln\left(d\right)$$

1

(AGB: Above Ground Biomass, d: $d_{1.30}$ diameter)

2.2.2. Image Processing and Satellite Dataset

In the study, Sentinel-2 satellite images of 26.05.2021–24.08.2021 and 22.11.2021 downloaded from NASA were used. A total of 10 bands were used for the analysis, including band 2, 3, 4, 5, 6, 7, 8, 8A, and 11 ve 12 from the satellite images of each date. Atmospheric correction was made on the images using ArcGIS software and the digital band values of the bands were converted to reflectance values and exported. Afterward, all bands were clipped according to the working limit and made ready for analysis. The analysis was carried out in two stages. In the first stage, buffer zones were discarded for each sample plot size (400, 600, and 800 m^2) from the sample plot centers in ArcGIS. The obtained sample plot polygons were overlapped with the bands of each date, and the digital band and reflectance values of each sample area were obtained with the “zonal statistics” command. In the second stage, some vegetation indices given in Table 3 were calculated separately for each date by using the reflectance values calculated for each band.

Table 3
Formulas of vegetation indices used in the analysis.

Vegetation Indices	Formula	Reference	Vegetation Indices	Formula	Reference
SAVI (Soil Adjusted Vegetation Index)	(B08 - B04) / (B08 + B04 + L) x (1.0 + L); L = 0.428	Huete (1988)	EVI2 (Enhanced Vegetation indices 2)	2.4 x (B08 - B04) / (B08 + B04 + 1.0)	Jiang *et al.* (2008)
PSSR (Pigment Specific Simple Ratio)	(B08 / B04)	Blackburn (1998)	CHL-RED-EDGE (Chlorophyll Red-Edge)	(B07 / B05) -1	Gitelson *et al.* (2005)
NDWI (Normalized Difference Water Index)	(B08-B11) / (B08 + B11)	McFeeters (1996)	ARI1 (Anthocyanin Reflectance Index)	(1.0 / B03–1.0 / B05)	Gitelson *et al.* (2001)
NDVI (Normalized Difference Vegetation Index)	(B08 - B04) / (B08 + B04)	Rouse *et al.* (1974)	BNDVI (Blue-normalized difference vegetation index)	(B08 - B02) / (B08 + B02)	Wang *et al.* (2007)
NBR (Normalized Burn Ratio)	(B08 - B12) / (B08 + B12)	Key and Benson (2006)	MNDVI (Modified Normalized Difference Vegetation Index)	(B08 - B12) / (B08 + B12)	Jurgens (1997)
MSI (Moisture Stress Index)	(B11 / B08)	Hunt and Rock (1989)	GBNDVI (Green-Blue NDVI)	(B08 - (B03 + B02)) / (B08 + (B03 + B02))	Wang *et al.* (2007)
MCARI (Modified Chlorophyll Absorption in Reflectance Index)	((B05 - B04) − 0.2 x (B05 - B03)) x (B05 / B04)	Haboudane *et al.* (2004)	GRNDVI (Green-Red NDVI)	(B08 - (B03 + B04)) / (B08 + (B03 + B04))	Gitelson and Merzlyak (1996)
GNDVI (Green Normalized Difference Vegetation Index)	(B08 - B03) / (B08 + B03)	Gitelson *et al.* (1996)	MCARI (Modified Chlorophyll Absorption in Reflectance Index)	((B05-B04)-0,2x(B06-B03))x(B05/B04)	Daughtry *et al.* (2000)
EVI (Enhanced Vegetation Index)	2.5 x (B08 - B04) / ((B08 + 6.0 x B04–7.5 x B02) + 1.0)	Liu and Huete (1995)	DVI (Difference Vegetation Index)	(B08 / B04)	Tucker (1980)
MSR (Modified Simple Ratio)	(B08 - B01) / (B04 - B01)	Chen (1996)	WDRVI (Wide Dynamic Range Vegetation Index)	(0.1 x B08 - B04) / (0.1 x B08 + B04)	Wang *et al.* (2007)
WDVI (Weighted Difference Vegetation Index)	(B08 - a x B04); a = 0.460	Clevers (1989)	GVMI (Global Vegetation Moisture Index)	((B08 + 0.1) - (B12 + 0.02)) / ((B08 + 0.1) + (B12 + 0.02))	Ceccato *et al.* (2002)
NLI (Nonlinear vegetation index)	(($B08^2$) - B04)) / (($B08^2$) + B04))	Goel and Qin (1994)	GARI (Green atmospherically resistant vegetation index)	(B08 - (B03 - (B02 - B04))) / (B08 - (B03 + (B02 - B04)))	Gitelson *et al.* (1996)

Vegetation Indices	Formula	Reference	Vegetation Indices	Formula	Reference
CCCI (Canopy Chlorophyll Content Index)	((B08 - B05) / (B08 + B05)) / ((B08 - B04) / (B08 + B04))	Fitzgerald *et al.* (2010)	GLI (Green leaf index)	(2.0 x B03 - B04 - B02) / (2.0 x B03 + B04 + B02)	Louhaichi *et al.* (2001)
ChlGreen (Chlorophyll Green)	(B07 / B03) -1	Gitelson *et al.* (2003)	GOSAVI (Green Optimized Soil Adjusted Vegetation Index)	(B08 - B03) / (B08 + B03 + Y); Y = 0,723	Rondeaux *et al.* (1996)
Clrededge (Chlorophyll IndexRedEdge)	(B08 / B05) – 1.0	Gitelson *et al.* (2003)	GSAVI (Green Soil Adjusted Vegetation Index)	(B08 - B03) / (B08 + B03 + L) x (1.0 + L); Y = 0,752	Sripada (2005)
CVI (Chlorophyll vegetation index)	B08 x (B04 / $B03^2$)	Vincini *et al.* (2007)	LCI (Leaf Chlorophyll Index)	(B08 - B05) / (B08 + B04)	Thenkabail *et al.* (1999)
CTVI (Corrected Transformed Vegetation Index)	(NDVI + 0,5) / abs(NDVI + 0,5) x sqrt(abs(NDVI + 0,5))	Perry *et al.* (1984)	PVR (Photosynthetic Vigour Ratio)	(B03 - B04) / (B03 + B04)	Metternicht (2003)

In the Sentinel-1A image, digital band, backscatter, and reflection values in different polarization (VV/VH) were obtained from VV and VH bands. Before the value calculations, some preprocessing was performed on the Sentinel-1 satellite image using SNAP software. These processes include thermal noise removal, calibration, and filtering. The bands prepared for analysis were overlapped with the sample areas and the digital band, backscatter, and reflectance values in different polarization (VV/VH) for each sample area were calculated with the “zonal statistics” command. Finally, using the digital elevation model obtained from the ALOS-PALSAR satellite image, the elevation, slope (%), and aspect (degrees) values of the working boundary were calculated with ArcGIS software. The obtained data were overlapped with the sample plots and the elevation, slope (%), and aspect (degree) values of each sample plot were obtained with the "zonal statistics" command. The datasets obtained with the remote sensing data for the sample areas individually and by the combination of these data are shown in Table 4.

Table 4
Datasets created with remote sensing data for modeling

Model Number	Dataset	Dataset Abbreviations
1	May (MAY) Sentinel-2 (S2) bant values (BV)	MAY_S2_BV
2	MAY Sentinel-2 reflectance values (REF)	MAY_S2_REF
3	MAY Sentinel-2 vegetation indices (VEG)	MAY_S2_VEG
4	MAY Sentinel-2 reflectance values and vegetation indices	MAY_S2_REF_VEG
5	MAY Sentinel-2 reflectance values, vegetation indices, Sentinel-1 (S1)(VV/VH) reflections values (REF)	MAY_S2_REF_VEG&S1_REF&TOP
6	MAY Sentinel-2 bant values and topographical data (TOP)	MAY_S2_BV&TOP
7	MAY Sentinel-2 reflectance values and topographical data	MAY_S2_REF&TOP
8	MAY Sentinel-2 vegetation indices and topographical data	MAY_S2_VEG&TOP
9	Sentinel-1 bant values (VV, VH)(BV), backscatter values (dB) and reflections values	S1_BV_dB_REF
10	Sentinel-1 bant values, backscatter values, reflections values, and topographical data	S1_BV_Db_REF&TOP
11	May Sentinel-2 reflectance values, vegetation indices, Sentinel-1 reflections values, and topographical data	MAY_S2_REF_VEG&S1_dB&TOP
12	August (AUG) Sentinel-2 bant values	AUG_S2_BV
13	AUG Sentinel-2 reflectance values	AUG_S2_REF
14	AUG Sentinel-2 vegetation indices	AUG_S2_VEG
15	AUG Sentinel-2 reflectance values and vegetation indices	AUG_S2_REF_VEG
16	AUG Sentinel-2 reflectance values, vegetation indices, Sentinel-1 reflections values, and topographical data	AUG_S2_REF_VEG&S1_REF&TOP
17	AUG Sentinel-2 bant values and topographical data	AUG_S2_BV&TOP
18	AUG Sentinel-2 reflectance values and topographical data	AUG_S2_REF&TOP
19	AUG Sentinel-2 vegetation indices and topographical data	AUG_S2_VEG&TOP
20	AUG Sentinel-2 reflectance values and vegetation indices, SENTİNEL-1 backscatter values, topographical data	AUG_S2_REF_VEG&S1_dB&TOP
21	AUG Sentinel-2 reflectance values,SENTİNEL-1 backscatter values, Sentinel-1 reflections values	AUG_S2_REF&S1_dB_REF
22	November (NOV) Sentinel-2 bant values	NOV_S2_BV
23	NOV Sentinel-2 reflectance values	NOV_S2_REF
24	NOV Sentinel-2 vegetation indices	NOV_S2_VEG
25	NOV Sentinel-2 reflectance values and vegetation indices	NOV_S2_REF_VEG
26	NOV Sentinel-2 reflectance values, vegetation indices, Sentinel-1 reflections values, topographical data	NOV_S2_REF_VEG&S1_REF&TOP
27	NOV Sentinel-2 bant values and topographical data	NOV_S2_BV&TOP
28	NOV Sentinel-2 reflectance values and topographical data	NOV_S2_REF&TOP
29	NOV Sentinel-2 vegetation indices and topographical data	NOV_S2_VEG&TOP
30	NOV Sentinel-2 reflectance values, vegetation indices, SENTİNEL-1 backscatter values, and topographical data	NOV_S2_REF_VEG&S1_dB&TOP
31	NOV Sentinel-2 reflectance values,SENTİNEL-1 backscatter values, Sentinel-1 reflections values and Sentinel-1 bant values	NOV_S2_REF&S1_dB_REF_BV

Model Number	Dataset	Dataset Abbrevıatıons
32	MAY Sentinel-2 reflectance values, vegetation indices, Sentinel-1 (S1)(VV/VH) reflections values (REF), AUG Sentinel-2 reflectance values, vegetation indices	MAY_S2_REF_VEG&S1_REF&TOP, AUG_S2_REF_VEG
33	MAY Sentinel-2 reflectance values, vegetation indices, Sentinel-1 (S1)(VV/VH) reflections values (REF) and topographical data, AUG Sentinel-2 reflectance values, vegetation indices, NOV Sentinel-2 reflectance values, vegetation indices, SENTİNEL-1 backscatter values,	MAY_S2_REF_VEG&S1_REF&TOP, AUG_S2_REF_VEG, NOV_S2_REF_VEG&S1_dB

2.2.3. Statistical Analysis Process

Digital band, band reflectance, and vegetation indices values obtained from Sentinel-2 satellite images taken in three different seasons were used in the development of models that predict the amount of above-ground biomass. In addition, digital band, band reflection, and backscatter values obtained from both polarizations of Sentinel-1A satellite image, and topographic (elevation, slope (%) and aspect (degrees)) data obtained from ALOS-PALSAR satellite were used. A total of 4,480.00 (20×224) data were generated from Sentinel-2 digital band (10 pieces) and band reflectance (10 pieces) values for all sample areas. Since these data were produced separately for each season, a total of 13,440 (4,480.00×3) digital tape and reflectance data were used. From the reflectance values, a total of 35 different vegetation indices values were calculated for each season image. In the general total (35×3×224), 23,520 vegetation indices values were used. Using a total of five data from Sentinel-1A and three topographically different data (8×224), a total of 1,792.00 data were used. In general, 38,752.00 pieces of data were used in the modeling of AGB. Advanced multiple linear regression method (MLR) was used to determine the linear relationship between AGB (dependent variable) and independent variables (Table 4) (Egual 2). SPSS software was used for the MLR algorithm. In the MLR method, backward is used in the selection of meaningful parameters. In the study, 80% (179) of 224 sample point data were used in the creation of the models and 20% (45) were used in testing the suitability of the models.

$$AGB = \beta_0 + \beta_1 . X_1 + \beta_2 . X_2 + \cdots + \beta_n . X_n + \epsilon$$

2

2.2.4. Performance Criteria

Different criteria were used to compare the estimation results using the observation data and modeling techniques obtained through the inventory study. In the study, coefficient of determination (R^2, Equal 3), mean absolute error (MAE, Equal 4), root mean square error (RMSE, Equal 5), Akaike criterion (AIC, Equal 6) and Bayesian information criterion (BIC, Equal 7) performance criteria were used. For the model to be successful, it is expected that the R^2 values will be large and the MAE, RMSE, BIAS, AIC, and BIC values should be small. Considering the performance criteria calculated for each parameter, a method that is successful according to one criterion may fail according to another criterion value. For this reason, a success ranking was made to cover all success criteria. For this purpose, the relative ranking method proposed by Poudel and Cao (2013) was used (R_j, equal 8). In this success ranking method, models are ranked relative to each other according to the closeness and distance values of the success criterion. Relative sequence numbers related to different criteria values were collected and the model with the smallest total relative sequence number was determined as the most successful for the relevant parameter (Özdemir, 2018; Ercanlı et al. 2018). The formulation of the performance criteria is shown in Table 5. Paired t-test was used to test the suitability of the models.

Table 5
Formulas of performance criteria

$R^2 = 1 - \frac{\sum_{i=1}^{n}(y_g - y_t)^2}{\sum_{i=1}^{n}(y_g - y_{og})^2}$	**(3)**
$MAE = \frac{1}{n}\sum_{i=1}^{n} \lvert h_i \rvert$	(4)
$RMSE = \sqrt{\frac{1}{n}\sum_{i=1}^{n}(h_i)^2}$	(5)
$AIC = \ln(RMSE) + 2k$	(6)
$BIC = \ln(RMSE) + \ln(k)$	(7)
$R_i = 1 + \frac{(m-1)x(S_i - S_{min})}{(S_{max} - S_{min})}$	(8)
*h: Residual, X: Primary variable, Y: Secondary variable, y_g: Observed, y_t: Predicted y_{og}: mean observation, n: sample count, k: Parameter in the model, m: Number of significant arguments, S_i: statistical criterion value, S_{min}: Minimum success criterion value for methods, S_{max}: Maximum success criterion value for methods	

3. Result

3.1. Descriptive statistics of datasets

AGB was calculated in a total of 224 sample plots. The average AGB of the sample plots is 86,950 ton ha^{-1}, the maximum and minimum AGB were calculated as 214,515 ton ha^{-1} and 12,097 ton ha^{-1}, respectively (Table 6). The minimum, maximum and mean AGB values of the training data were found to be 12.097, 214.515, and 88.387 ton ha^{-1}, respectively. Finally, in the validation data set, the mean AGB was found to be 81.237 tons ha^{-1}. The fact that the mean AGB of all data sets are close to each other shows that the data separation is done in a balanced way.

Table 6
Descriptive statistical AGB (ton ha^{-1}) values for total, training, and validation data

Data	N	Min.	Max.	Mean	Std. D
Total AGB	224	12.097	214.515	86.950	32.861
Training AGB	179	12.097	214.515	88.387	33.843
Validation AGB	45	35.080	175.427	81.237	28.242

3.2. Multi-linear regression (MLR) model results

In the study, AGB was modeled by the MLR method using datasets consisting of vegetation indices, digital band, and reflectance values obtained from Sentinel-2 satellite images taken in rainy, semi-arid, and dry seasons. Likewise, reflection, backscatter, and polarization data sets obtained from Sentinel-1 for sample areas were also used with topographic datasets. A total of 33 models were obtained with individual and combinations of all these datasets. The performances of the models were checked with a coefficient of determination (R^2), root mean square error (RMSE), mean absolute error (MAE), akaike information criterion (AIC), and Bayesian information criterion (BIC). The most successful model was determined not based on a single performance criterion, but by the relative ranking method (R_j), which evaluates all performance criteria jointly. Model performance measures related to training datasets are shown in Table 7, and model performance measures related to validation datasets are shown in Table 8.

Table 7
Model performance criteria related to training data sets

No	Auxiliary variable (data set)	Performance Criteria					Relative Rank					
		R^2	RMSE	MAE	BİC	AİC	R^2	RMSE	MAE	BİC	AİC	TOTAL RANK
1	MAY_S2_BV	0.27	31.26	26.97	4.60	9.50	17.25	9.63	16.32	9.64	4.84	57.68
2	MAY_S2_REF	0.21	31.99	23.85	4.88	11.50	21.00	10.30	11.66	13.68	7.02	63.66
3	MAY_S2_VEG	0.2	25.64	19.45	5.91	27.42	21.63	4.54	5.09	28.48	24.48	84.21
4	MAY_S2_REF_VEG	0.19	30.50	23.23	5.98	29.42	22.25	8.95	10.74	29.57	26.66	98.16
5	MAY_S2_REF_VEG&S1_REF&TOP	0.27	29.20	22.24	6.08	33.37	17.25	7.76	9.26	31.00	31.00	96.27
6	MAY_S2_BV&TOP	0.33	21.74	16.72	4.84	11.46	33.50	1.00	1.00	23.12	6.98	65.60
7	MAY_S2_REF&TOP	0.29	29.85	22.88	5.38	17.44	16.00	8.36	10.22	20.91	13.53	69.01
8	MAY_S2_VEG&TOP	0.29	29.85	22.88	5.96	29.40	16.00	8.36	10.22	29.25	26.64	90.47
9	S1_BV_dB_REF	0.05	54.82	36.78	4.00	6.00	31.00	31.00	31.00	1.00	1.00	95.00
10	S1_BV_Db_REF&TOP	0.18	30.50	23.03	5.62	21.42	22.88	8.95	10.44	24.26	17.89	84.41
11	MAY_S2_REF_VEG&S1_dB&TOP	0.22	29.49	21.03	5.58	21.38	20.38	8.03	7.44	23.77	17.86	77.48
12	AUG_S2_BV	0.12	33.07	25.18	4.60	9.50	26.63	11.28	13.65	9.56	4.83	65.94
13	AUG_S2_REF	0.15	32.73	24.82	4.87	11.49	24.75	10.97	13.11	13.57	7.01	69.40
14	AUG_S2_VEG	0.21	32.50	24.77	4.87	11.48	21.00	10.76	13.03	13.47	7.00	65.27
15	AUG_S2_REF_VEG	0.23	31.07	23.71	5.63	21.44	19.75	9.46	11.46	24.52	17.92	83.11
16	AUG_S2_REF_VEG&S1_REF&TOP	0.31	29.20	22.20	5.94	29.37	14.75	7.76	9.20	28.93	26.62	87.26
17	AUG_S2_BV&TOP	0.18	31.05	23.73	5.23	15.44	22.88	9.45	11.48	18.66	11.34	73.80
18	AUG_S2_REF&TOP	0.21	30.70	23.31	5.37	17.42	21.00	9.13	10.86	20.72	13.52	75.22
19	AUG_S2_VEG&TOP	0.23	29.82	22.57	5.70	23.40	19.75	8.33	9.75	25.45	20.06	83.35
20	AUG_S2_REF_VEG&S1_dB&TOP	0.27	29.59	22.81	5.87	27.39	17.25	8.12	10.11	27.97	24.44	87.89
21	AUG_S2_REF&S1_dB_REF	0.08	32.73	24.82	4.87	11.49	29.13	10.97	13.11	13.57	7.01	73.78
22	NOV_S2_BV	0.07	33.34	25.18	4.20	7.51	29.75	11.52	13.65	3.83	2.65	61.40
23	NOV_S2_REF	0.11	33.35	25.35	4.20	7.51	27.25	11.53	13.90	3.83	2.65	59.15
24	NOV_S2_VEG	0.15	31.95	24.24	5.41	17.46	24.75	10.26	12.24	21.30	13.56	82.11
25	NOV_S2_REF_VEG	0.13	32.72	24.66	4.59	9.49	26.00	10.95	12.87	9.41	4.82	64.05
26	NOV_S2_REF_VEG&S1_REF&TOP	0.34	27.27	21.48	6.01	33.31	12.88	6.02	8.12	30.02	30.93	87.96
27	NOV_S2_BV&TOP	0.16	30.03	23.84	5.19	15.40	24.13	8.52	11.64	18.18	11.30	73.77
28	NOV_S2_REF&TOP	0.12	32.03	23.84	5.55	19.47	26.63	10.34	11.64	23.26	15.76	87.63
29	NOV_S2_VEG&TOP	0.3	28.73	21.67	5.76	25.36	15.38	7.34	8.41	26.29	22.21	79.62
30	NOV_S2_REF_VEG&S1_dB&TOP	0.35	27.88	21.62	5.73	25.33	12.25	6.57	8.33	25.85	22.18	75.18
31	NOV_S2_REF&S1_dB_REF_BV	0.06	32.95	24.98	4.59	9.49	30.38	11.16	13.36	9.51	4.83	69.23
32	MAY_S2_REF_VEG&S1_REF&TOP, AUG_S2_REF_VEG	0.49	26.21	22.50	5.42	21.23	3.50	5.05	9.64	21.50	17.69	57.38

S2: Sentinel-2, S1: Sentinel-1, AUG: August, NOV: November, BV: Bant value, REF: Reflectance, VEG: Vegetation indices, TOP: Topographical data, dB: Bant backscatter

No	Auxiliary variable (data set)	Performance Criteria					Relative Rank					
		R²	RMSE	MAE	BİC	AİC	R²	RMSE	MAE	BİC	AİC	TOTAL RANK
33	MAY_S2_REF_VEG&S1_REF&TOP, AUG_S2_REF_VEG, NOV_S2_REF_VEG&S1_dB	0.53	24.61	20.31	5.73	29.16	1.00	3.61	6.37	25.87	26.38	63.23

S2: Sentinel-2, S1: Sentinel-1, AUG: August, NOV: November, BV: Bant value, REF: Reflectance, VEG: Vegetation indices, TOP: Topographical data, dB: Bant backscatter

When the results of the training datasets were examined, the highest coefficient of determination (R^2 = 0.33) in the datasets obtained from the Sentinel-2 satellite image of the month of May (rainy) was obtained in model number 6, which was created from digital tape and topographic data (RMSE = 21.74 ton ha^{-1}, MAE = 16.72 ton ha^{-1}). After model 6 for May, the highest coefficient of determination (R^2 = 0.29) was obtained in models 7 and 8 of the datasets of vegetation index, reflectance data, and topographic data. The lowest coefficient of determination (R^2 = 0.19) for the month of May was obtained in model number 4. When the results of August (semi-arid) were examined, the highest coefficient of determination (R^2 = 0.31) was obtained in model number 16 belonging to the data set created with the vegetation indices values obtained from the Sentinel-2 satellite image, the reflectance and topographic data obtained from the Sentinel-1 satellite image (RMSE = 29.20 ton ha^{-1}, MAE = 22.20 ton ha^{-1}). The lowest coefficient of determination for August (R^2 = 0.08) was found in model 21, which consists of reflectance values obtained from the Sentinel-2 satellite image and reflectance and backscatter values obtained from the Sentinel-1 satellite image (RMSE = 32.73 ton ha^{-1}, MAE = 24.82 ton ha^{-1}). In the results of November (dry) month, the highest coefficient of determination (R^2 = 0.35), vegetation index, and reflectance values obtained from Sentinel-2 satellite image backscattering obtained from Sentinel-1 satellite image and topographic data were obtained in model number 30 (RMSE = 27.88 ton ha^{-1}, MAE = 21.62 ton ha^{-1}). After model number 30 for November, the highest coefficient of determination (R^2 = 0.34), vegetation index, and reflectance values obtained from the Sentinel-2 satellite image, reflectance obtained from Sentinel-1 satellite image, and model 26 belonging to topographic data were obtained (RMSE = 27.27 ton ha^{-1}, MAE = 21.48 ton ha^{-1}). The lowest coefficient of determination (R^2 = 0.06) for November was found in model 31, which consists of reflectance values obtained from the Sentinel-2 satellite image, reflectance, backscatter, and digital band values obtained from Sentinel-1 satellite image (RMSE = 32.95 ton ha^{-1}, MAE = 24.98 ton ha^{-1}). The digital band values of the Sentinel-2 satellite images for three different seasons and the May, August, and November coefficients of determination for the modeling of the AGB were found to be 0.27, 0.12, and 0.07, respectively. The highest coefficient of determination with digital band values was obtained in the rainy season R^2 = 0.27, RMSE = 31.26 ton ha^{-1}, MAE = 26.97 ton ha^{-1}). The reflectance values of the Sentinel-2 satellite images and the indication coefficients of the AGB modeling for May, August, and November were found to be 0.21, 0.15, and 0.11, respectively. As with the digital band values, the highest coefficient of determination in reflectance values was obtained in the rainy season (R^2 = 0.21, RMSE = 31.99 ton ha^{-1}, MAE = 23.85 ton ha^{-1}). In the modeling of the AGB using vegetation indices values obtained from Sentinel-2 satellite images, the coefficients of determination for May, August, and November were calculated as 0.20, 0.21, and 0.15, respectively. With vegetation indices values, the highest coefficient of determination was obtained in the semi-arid season (R^2 = 0.20, RMSE = 32.50 ton ha^{-1}, MAE = 24.77 ton ha^{-1}). It was determined that there was an increase in the coefficients of determination in the models obtained by adding topographic data to the data sets belonging to all periods. The digital band, reflectance, and vegetation indices values for May and the model indication coefficients in which topographic data were included in these values were found to be 0.27–0.33, 0.21–0.29, and 0.20–0.29, respectively. The digital band, reflectance, and vegetation indices values for August and the model indication coefficients in which topographic data were included in these values were found to be 0.12–0.18, 0.15–0.21, and 0.21–0.23, respectively. Finally, the digital band, reflectance, and vegetation indices values for November and the coefficients of determination in the models in which topographic data were included in these values were calculated as 0.07–0.16, 0.11–0.12, and 0.15–0.30, respectively. With the data set obtained with the digital band, reflectance, and backscatter values obtained from the Sentinel-1 satellite image, the model coefficient for the modeling of the AGB was found to be 0.05 (RMSE = 54.82 ton ha^{-1}, MAE = 36.78 ton ha^{-1}). As in Sentinel-2 data sets, it was observed that the coefficient of determination increased in the modeling made by adding topographic data to Sentinel-1 data (R^2 = 0.18, RMSE = 30.50 ton ha^{-1}, MAE = 23.03 ton ha^{-1}). The most successful model for Sentinel-2 May datasets was obtained from band reflectance values (R^2 = 0.20,

R_j=57.68). The most successful model, in which AGB was modeled with August data, was obtained in model 14 (R^2 = 0.21, R_j=65.27). The most successful model for November was obtained with the reflectance data obtained from the Sentinel-2 satellite image (R^2 = 0.20, R_j=59.15). In addition to all these data sets, a new dataset was obtained by combining the most successful data sets of each month and AGB was modeled (Models 32 and 33). The most successful model in which AGB is modeled with training datasets is 32 (R_j=57.38).

Table 8
Model performance criteria related to validation data sets

No	Auxiliary variable (data set)	Performance Criteria					Relative Rank					
		R^2	RMSE	MAE	BİC	AİC	R^2	RMSE	MAE	BİC	AİC	TOTAL RANK
1	MAY_S2_BV	0.23	28.20	19.74	4.39	11.01	22.21	22.09	18.65	17.18	4.63	84.75
2	MAY_S2_REF	0.18	22.77	18.12	4.13	9.03	24.79	13.62	15.28	13.90	3.41	71.00
3	MAY_S2_VEG	0.13	33.87	25.66	5.41	32.70	27.38	30.95	31.00	29.99	17.97	137.28
4	MAY_S2_REF_VEG	0.21	30.52	22.10	5.31	32.60	23.24	25.71	23.57	28.78	17.91	119.21
5	MAY_S2_REF_VEG&S1_REF&TOP	0.64	14.69	11.27	5.25	28.69	1.00	1.00	1.00	28.03	15.50	46.53
6	MAY_S2_BV&TOP	0.28	21.32	17.04	4.57	12.96	19.62	11.35	13.02	19.43	5.83	69.24
7	MAY_S2_REF&TOP	0.28	20.77	16.12	4.13	9.03	19.62	10.49	11.11	13.90	3.41	58.54
8	MAY_S2_VEG&TOP	0.48	17.25	14.43	4.79	16.85	9.28	4.99	7.59	22.24	8.22	52.31
9	S1_BV_dB_REF	0.06	23.73	20.67	3.17	5.17	31.00	15.12	20.60	1.72	1.04	69.48
10	S1_BV_Db_REF&TOP	0.1	24.52	20.87	3.89	7.20	28.93	16.35	21.02	10.88	2.29	79.46
11	MAY_S2_REF_VEG&S1_dB&TOP	0.21	31.18	23.48	5.14	28.58	23.24	26.75	26.44	26.66	15.44	118.53
12	AUG_S2_BV	0.16	22.50	18.74	3.11	5.11	25.83	13.20	16.56	1.05	1.00	57.64
13	AUG_S2_REF	0.17	22.41	18.59	3.11	5.11	25.31	13.05	16.25	1.00	1.00	56.62
14	AUG_S2_VEG	0.19	30.99	23.84	5.49	46.40	24.28	26.45	27.19	31.00	26.39	135.31
15	AUG_S2_REF_VEG	0.29	20.08	17.93	5.40	42.40	19.10	9.41	14.88	29.90	23.94	97.24
16	AUG_S2_REF_VEG&S1_REF&TOP	0.28	21.38	17.51	5.30	50.13	19.62	11.45	14.01	28.68	28.69	102.45
17	AUG_S2_BV&TOP	0.29	20.69	16.51	4.42	11.03	19.10	10.38	11.91	17.48	4.64	63.51
18	AUG_S2_REF&TOP	0.23	19.99	16.47	4.60	13.00	22.21	9.28	11.83	19.86	5.85	69.03
19	AUG_S2_VEG&TOP	0.18	30.48	23.50	5.27	36.44	24.79	25.66	26.49	28.30	20.27	125.52
20	AUG_S2_REF_VEG&S1_dB&TOP	0.26	28.59	21.80	5.14	53.89	20.66	22.70	22.95	26.66	31.00	123.96
21	AUG_S2_REF&S1_dB_REF	0.13	33.11	25.18	4.39	11.00	27.38	29.76	30.00	17.12	4.62	108.89
22	NOV_S2_BV	0.29	20.68	16.61	4.13	9.03	19.10	10.35	12.14	13.84	3.41	58.84
23	NOV_S2_REF	0.16	22.41	18.59	3.11	5.11	25.83	13.05	16.25	1.00	1.00	57.13
24	NOV_S2_VEG	0.12	32.99	24.84	5.39	46.30	27.90	29.57	29.28	29.80	26.34	142.87
25	NOV_S2_REF_VEG	0.14	32.08	23.93	5.49	42.49	26.86	28.15	27.39	30.99	23.99	137.38
26	NOV_S2_REF_VEG&S1_REF&TOP	0.27	28.08	23.45	5.20	22.89	20.14	21.91	26.38	27.34	11.94	107.71
27	NOV_S2_BV&TOP	0.38	19.32	15.62	4.35	10.96	14.45	8.23	10.06	16.62	4.60	53.96
28	NOV_S2_REF&TOP	0.4	18.90	15.05	4.55	12.94	13.41	7.57	8.87	19.15	5.82	54.82
29	NOV_S2_VEG&TOP	0.13	33.91	24.99	4.89	16.94	27.38	31.00	29.60	23.40	8.28	119.65
30	NOV_S2_REF_VEG&S1_dB&TOP	0.29	20.69	16.89	4.13	9.03	19.10	10.38	12.70	13.85	3.41	59.44
31	NOV_S2_REF&S1_dB_REF_BV	0.25	21.21	17.74	4.15	9.05	21.17	11.18	14.48	14.16	3.43	64.42
32	MAY_S2_REF_VEG&S1_REF&TOP, AUG_S2_REF_VEG	0.51	17.25	14.43	4.79	16.85	7.72	4.99	7.59	22.24	8.22	50.76

S2: Sentinel-2, S1: Sentinel-1, AUG: August, NOV: November, BV: Bant value, REF: Reflectance, VEG: Vegetation indices, TOP: Topographical data, dB: Bant backscatter

No	Auxiliary variable (data set)	Performance Criteria					Relative Rank					
		R^2	RMSE	MAE	BİC	AİC	R^2	RMSE	MAE	BİC	AİC	TOTAL RANK
33	MAY_S2_REF_VEG&S1_REF&TOP, AUG_S2_REF_VEG, NOV_S2_REF_VEG&S1_dB	0.51	25.21	21.50	5.36	21.16	7.72	17.42	22.32	29.38	10.87	87.71
S2: Sentinel-2, S1: Sentinel-1, AUG: August, NOV: November, BV: Bant value, REF: Reflectance, VEG: Vegetation indices, TOP: Topographical data, dB: Bant backscatter												

When the results of the validation datasets are examined, the highest coefficient of determination (R^2 = 0.48) in the datasets obtained from the Sentinel-2 satellite images of the month of May (rainy) was obtained in the model number 8 formed from the vegetation indices and topographic data (RMSE = 17.25 ton ha^{-1}, MAE = 14.43 ton ha^{-1}). The lowest coefficient of determination (R^2 = 0.13) for May was obtained in model number 3. When the results of the August (semi-arid) month are examined, the highest coefficient of determination (R^2 = 0.29) is obtained in the 15 and 17th models created with vegetation indices and reflectance values obtained from the Sentinel-2 satellite image and the band reflection obtained from the Sentinel-1 satellite image and topographic (RMSE = 20.08–20.69 ton ha^{-1}, MAE = 17.93–16.51 ton ha^{-1}). The lowest coefficient of determination for August (R^2 = 0.13) was obtained in model number 21, which was created with the reflectance values obtained from the Sentinel-2 satellite image and the reflectance and backscatter values obtained from the Sentinel-1 satellite image (RMSE = 33.11 ton ha^{-1}, MAE = 25.18 ton ha^{-1}). The high coefficient of determination (R^2 = 0.40) for the month of November (dry) was obtained in model number 28, which was created from topographic data with the reflectance obtained from the Sentinel-2 satellite image (RMSE = 18.90 ton ha^{-1}, MAE = 15.05 ton ha^{-1}). The lowest coefficient of determination (R^2 = 0.12) for November was obtained in model 24. For modeling of AGB with digital band values obtained from Sentinel-2 satellite images of three different seasons, the coefficients of determination for May, August, and November were found to be 0.23, 0.16, and 0.29, respectively. The highest coefficient of determination with validation digital band values was obtained in the dry season (R^2 = 0.29, RMSE = 20.68 ton ha^{-1}, MAE = 16.61 ton ha^{-1}). For the Validation AGB models, the reflectance values obtained from Sentinel-2 satellite images and the coefficients of determination for May, August, and November were found to be 0.18, 0.17, and 0.16, respectively. The highest coefficient of determination with reflectance data was obtained in the rainy season (R^2 = 0.18, RMSE = 22.77 ton ha^{-1}, MAE = 18.12 ton ha^{-1}). The vegetation indices values obtained from Sentinel-2 satellite images and the coefficients of determination for May, August, and November of the AGB models were calculated as 0.13, 0.19, and 0.12, respectively. It was determined that there was an increase in the coefficients of determination in the models obtained by adding topographic data to the data sets belonging to all periods. Sentinel-2 digital band, reflectance, and vegetation indices values for May and model indication coefficients in which topographic data were included in these values were found to be 0.23–0.28, 0.18–0.28, and 0.13–0.48, respectively. The digital band, reflectance, and vegetation indices values for August and the model indication coefficients in which topographic data were included in these values were found to be 0.16–0.29, 0.17–0.23, and 0.19 – 0.18, respectively. Finally, when the digital band, reflectance, and vegetation indices values for November and the models in which topographic data were included in these values were examined, the coefficients of determination were calculated as 0.29–0.38, 0.16–0.40 and 0.12–0.13, respectively. With the data set obtained from the digital band, reflectance, and backscatter values obtained from the Sentinel-1 satellite image, the model specification coefficient for the modeling of the AGB was found to be 0.06 (RMSE = 23.73 ton ha^{-1}, MAE = 20.67 ton ha^{-1}). It was observed that the coefficient of determination increased in the modeling made with the addition of topographic data to the Sentinel-1 data (R^2 = 0.10, RMSE = 31.18 ton ha^{-1}, MAE = 23.48 ton ha^{-1}). In Sentinel-2 May datasets, the most successful model was obtained from reflectance values (R^2 = 0.18, R_j=71.00). The most successful model, in which AGB was modeled with August data, is model number 13 (R^2 = 0.17, R_j=56.62). The most successful model for November was obtained with the reflectance data obtained from the Sentinel-2 satellite image (R^2 = 0.16, R_j=57.13). In addition to all these datasets, a new dataset was obtained by combining the most successful datasets of each month, and the AGB was modeled (Models 32 and 33). The most successful model for which AGB is modeled for validation is 32 (R_j=50.76).

3.3. The most successful model results for AGB

The study obtained the highest success in modeling AGB in model 32 (R_j=57.38). The model includes the reflectance and vegetation indices values obtained from the Sentinel-2 satellite image of May and August, the reflectance values obtained from the Sentinel-1 satellite image, and the variables consisting of topographic values. In addition, to more clearly show the success levels of the 33 different regression models developed, the model's total relative rank and coefficients of expression are shown in Fig. 3.

When Fig. 3 is examined, the model with the lowest total relative rank is 32, and the most successful model obtained later is model number 1. Although model number 1 had a low coefficient of determination, it was determined that it was the second most successful model in total relative order. In general model results, it is expected that other criteria (RMSE, MAE, BIC, and AIC) with a high coefficient of determination will be low. It is thought that an evaluation based on a single performance criterion in the selection of the most successful model will be misleading. The variation of the above-ground biomass estimated in the most successful model No. 32 compared to the above-ground biomass calculated from the inventory scorecards and the distribution of errors are as shown in Fig. 4.

When Fig. 4 is examined, it is seen that the forecast and observation data exhibit a normal distribution (a), and the error terms of the model show a normal distribution according to the estimated surface biomass (b). The training performance criteria of model 32 were calculated as R^2, RMSE, MAE, BIC, and AIC as 0.49, 26.21, 22.50, 5.42, and 21.23, respectively. The validation performance criteria of model 32 were calculated as R^2, RMSE, MAE, BIC, and AIC, respectively, 0.51, 17.45, 14.43, 4.79, and 16.85. In addition, the model's training and validation Taylor diagrams are shown in Fig. 5 to more clearly show the performance criteria of the most successful model number 32. The results of the most successful model (32) variables are shown in Table 9. The statistical fit of Model 32 was tested with an independent dataset using a paired-sample t-test. The test results in question (t = 0.473 and p = 0.639) showed that Model 32 was suitable and usable for modeling AGB.

Table 9
Model results that best predict aboveground biomass

Independent variables	Coefficients	Std. Error	t	*p-value*
(Constant)	-968.725	288.632	-3.356	0.001
MAY_B02	-1215.763	558.896	-2.175	0.031
MAY_B07	973.124	274.627	3.543	0.001
MAY_PSSR	-1.598	0.483	-3.310	0.001
MAY_MCARI	78.604	23.386	3.361	0.001
MAY_CHL-R-E	578.582	226.919	2.550	0.012
MAY_CCCI	244.865	145.778	1.680	0.045
MAY_GARI	669.357	220.032	3.042	0.003
MAY_LCI	200.275	70.907	2.824	0.005
MAY_SARVI	-1055.022	295.310	-3.573	0.000
VV/VH	2.465	1.192	2.068	0.040
ELEVATION	0.928	0.232	3.999	0.000
AUG_B05	-1386.694	402.364	-3.446	0.001
AUG_B12	733.849	184.200	3.984	0.000
AUG_NDVI	-164.542	47.349	-3.475	0.001
AUG_BNDVI	62.709	18.825	3.331	0.001
AUG_SAVI	710.133	158.902	4.469	0.000
AUG_GOSAVI	-1073.726	343.555	-3.125	0.002

MAY: May, AUG: August, PSSR: Pigment Specific Simple Ratio, MCARI: Modified Chlorophyll Absorption in Reflectance Index, CHL_R_E: Chlorophyll Red-Edge, CCCI: Canopy Chlorophyll Content Index, GARI: Green atmospherically resistant vegetation index, LCI: Leaf Chlorophyll Index, SARVI: Soil and Atmospherically Resistant Vegetation Index, NDVI: Normalized Difference Vegetation Index, BNDVI: Blue-normalized difference vegetation index, SAVI: Soil Adjusted Vegetation Index, GOSAVI: Green Optimized Soil Adjusted Vegetation Index.

4. Discussion

4.1. Comparison of S1 and S2 satellite images on modeling AGB

In the modeling of the AGB, the data sets of digital band, reflectance, and vegetation indices values obtained from Sentinel-2 (passive) satellite image were compared to the dataset of the digital band, reflectance and backscatter values obtained from Sentinel-1 (active) proved to be more appropriate and successful. In some studies where active and passive images were compared in the modeling of AGB (Vafaei et al., 2018; Zhao et al., 2016; Forkuor et al., 2020), they reached the same conclusion. In addition, there are studies in which active images yield better results than passive images in modeling AGB (exp. Chen et al., 2018; Navarro et al. 2019; Günlü and Ercanlı, 2020). In general, it is seen that active images show lower success than passive images in modeling AGB. The main reason for this situation is thought to have a limiting effect in terms of S1 (C-band) short wavelength modeling. Because C-band has limited penetration ability into vegetation. It is thought that using longer wavelength active image bands (exp. L and P) in modeling AGB will increase the success of the model. Another reason is thought to be because the number of data obtained from Sentinel-2 is higher than the number of data obtained from Sentinel-1. It is seen that the success of the model increases as the number of variables in the modeling increases. To increase the number of data to be obtained from Sentinel-1, it has been observed that the success has increased with the calculation of different index values and including them in the modeling (Laurin et al., 2018; Forkuor et al., 2020). In a study where AGB was modeled using Sentinel-1 time series, it was seen that the use of time series also increased the modeling success (Santoro et al., 2013; Laurin et al., 2018). In addition, it is predicted that the integration of SAR data obtained from longer wavelengths (exp. L and P band) with Sentinel-1 and Sentinel-2 in modeling AGB with passive images can reduce the limiting effect of C-band and improve the accuracy of AGB modeling (Laurin et al., 2018). In the study by Nuthammachot et al. (2022), the AGB was modeled separately with three data sets created by the integration of Sentinel-1, Sentinel-2, and Sentinel-1 and Sentinel-2 data using the variables obtained from Sentinel-1 and Sentinel-2 satellite images. The models' determination coefficients were obtained as 0.34, 0.82, and 0.84, respectively. The results showed that data integration had a positive effect on model success.

4.2. Combination of Sentinel satellite images and topographic data on modeling the AGB

In the study, it was seen that more successful models were obtained with the combination of data sets obtained from Sentinel-1 and Sentinel-2 satellite images (Table 6). Especially in this study, the highest success in modeling AGB was obtained in the data set consisting of reflectance and vegetation indices values obtained from the Sentinel-2 satellite image, reflectance (VV/VH) obtained from the Sentinel-1 satellite image, and topographic data (R^2 = 0.49, RMSE = 26.21, MAE = 22.50, BIC = 5.42, AIC = 21.23). While modeling the AGB using only Sentinel-1 data, a coefficient of determination of 0.05 was obtained, it was observed that the coefficient of determination increased to 0.18 when topographic data were included in these data (Table 6). It was observed that the modeling success increased with the inclusion of topographic data in the data obtained from Sentinel-2 satellite images. For example, in the study, the coefficients of indication for Sentinel-2 digital band, reflectance, and vegetation indices values for May, and for the models in which topographic data were included in these values, were found to be 0.27–0.33, 0.21–0.29 and 0.20–0.29, respectively. Similar to our study, Baloloy et al. (2018) stated that they achieved higher success with the combination of the Sentinel-2, Planet scope, and RapidE images and the data obtained from the images in which the forest AGB was modeled. Kumar et al. (2016) tried to model AGB using Landsat 8 OLI and Alos-2 satellite images. The model coefficients of the data sets created from the combination of Landsat 8, Alos-2, and Landsat and Alos-2 were obtained as 0.78, 0.74, and 0.85, respectively. Keleş et al. (2021), tried to estimate the aboveground stand carbon in pure Scotch pine stands using Sentinel-1 and Sentinel-2 satellite images, and they concluded that the use of two satellite images together increased the modeling success. It is seen that similar results were obtained in another study by Bulut (2023). In general, the production of data sets with the combination of data from Sentinel-1 and Sentinel-2 satellite images in the modeling of AGB increased the modeling success. In addition to these, it was seen that even more successful models could be obtained by adding topographic data to the datasets.

4.3. The effect of seasonality on AGB modeling

In the study, AGB was modeled separately with the digital band, reflectance, and vegetation indices values obtained from Sentinel-2 satellite images for May (rainy), August (semi-arid), and November (dry). The model coefficients in which the AGB is modeled using the digital band values of May, August, and November are 0.27, 0.12, and 0.07, respectively. The coefficients of determination for the reflectance values were calculated as 0.21, 0.15, and 0.11. Finally, the coefficients of indication for vegetation indices values were calculated as 0.20, 0.21, and 0.15. Although the same datasets obtained from the Sentinel-2 satellite image were used in all periods, the differences in the results show the effect of seasonality on the models. The higher model performances in the rainy month are thought to be related to higher vegetation during the rainy season and thus better correlation with remotely sensed data. It has been stated in some studies that seasonality is also effective in modeling, especially in short wavelength (Sentinel-1) satellite images. It is stated that the use of dry season images of active, short wavelength, and low penetration satellites will increase the success of the modeling (Vaglio Laurin et al., 2013). Likewise, Nguyen et al. (2016) obtained similar results in modeling AGB with ALOS-2 data. Forkuor et al. (2020) obtained similar results in their study in which they tried to model the AGB with Sentinel-1 and Sentinel-2 satellite images in different seasons and stated that more successful models would be obtained with Sentinel-1 images belonging to the dry season.

5. Conclusion

In this study, AGB of pure Calabrian pine (*Pinus brutia* Ten.) stands were tried to be modeled using Sentinel-2 time series and Sentinel-1 satellite images and topographic data. Digital band, reflectance, and vegetation indices values from the Sentinel-2 satellite image, and digital band, reflectance, and backscatter values from the Sentinel-1 satellite image were used. The results were checked with the relative rank method, which takes into account all performance criteria. The highest success in the individual modeling of the data was obtained in the digital band values obtained from the Sentinel-2 satellite image of May (May_BV, R^2 = 0.27). It was observed that the success rate increased in the models made with the integration of topographic data into all data sets (May_BV&TOP, R^2 = 0.33). The highest success in the study was obtained in the model made with the combination of all data (Model 32, R^2 = 0.49). In the study, it was determined that the combination of data had an improving effect on modeling success. It is thought that the application of different modeling techniques (artificial neural networks, support vector machine, random forest method) in future studies can increase the model success of AGB. However, it is thought that the use of images with longer wavelengths and high penetration to increase the model success of active satellite images can increase the model success of AGB. It is thought that modeling success can be increased with LIDAR technologies that can be integrated into unmanned aerial vehicles recently.

Declarations

Author contributions

The entire study was prepared by Hasan AKSOY. There is no conflict of interest.

Data availability

The authors do not have permission to share data.

Funding

No funding was obtained for this study

References

1. Anonim (2021). Orman Genel Müdürlüğü, Serik Orman Amenajman Planı 2021-2031. Antalya Orman Bölge Müdürlüğü, Ankara: OGM.
2. Baloloy, A. B., Blanco, A. C., Candido, C. G., Argamosa, R. J. L., Dumalag, J. B. L. C., Dimapilis, L. L. C., & Paringit, E. C. (2018). Estimation of mangrove forest aboveground biomass using multispectral bands, vegetation indices, and biophysical variables derived from optical satellite imageries: Rapideye, planetscope, and sentinel-2. ISPRS annals of the photogrammetry, remote sensing and spatial information sciences, 4, 29-36. https://doi.org/10.5194/isprs-annals-IV-3-29-2018
3. Berninger, A., Lohberger, S., Zhang, D., & Siegert, F. (2019). Canopy height and above-ground biomass retrieval in tropical forests using multi-pass X-and C-bant Pol-InSAR data. Remote Sensing, 11(18), 2105. https://doi.org/10.3390/rs11182105
4. Blackburn, G. A. (1998). Spectral indices for estimating photosynthetic pigment concentrations: a test using senescent tree leaves. International Journal of Remote Sensing, 19(4): 657-675. https://doi.org/10.1080/014311698215919
5. Brown, S. (2002). Measuring carbon in forests: current status and future challenges. Environmental Pollution, 116(3): 363-372. https://doi.org/10.1016/S0269-7491(01)00212-3
6. Brown, S. and Iverson, L.R. (1992). Biomass estimates for tropical forests. World Resource Review, 4 (3): 366-384.
7. Bulut, S. (2023). Machine learning prediction of above-ground biomass in pure Calabrian pine (Pinus brutia Ten.) stands of the Mediterranean region, Türkiye. Ecological Informatics, 74, 101951. https://doi.org/10.1016/j.ecoinf.2022.101951
8. Ceccato, P., Gobron, N., Flasse, S., Pinty, B. and Tarantola, S. 2002. Designing a spectral index to estimate vegetation water content from remote sensing data: Part 1: Theoretical approach. Remote Sensing of Environment, 82(2-3), 188-197. https://doi.org/10.1016/S0034-4257(02)00037-8
9. Chen, J.M. 1996. Evaluation of vegetation indices and a modified simple ratio for boreal applications. Canadian Journal of Remote Sensing, 22(3), 229-242. https://doi.org/10.1080/07038992.1996.10855178
10. Chen, L., Ren, C., Zhang, B., Wang, Z., & Xi, Y. (2018). Estimation of forest above-ground biomass by geographically weighted regression and machine learning with sentinel imagery. Forests, 9(10), 582. https://doi.org/10.3390/f9100582
11. Clevers, J.G.P.W. 1989. Application of a weighted infrared-red vegetation indices for estimating leaf area index by correcting for soil moisture. Remote Sensing of Environment, 29(1), 25-37. https://doi.org/10.1016/0034-4257(89)90076-X
12. Crippen, R.E. (1990). Calculating the vegetation indices faster. Remote Sensing of Environment, 34, 71–73. https://doi.org/10.1016/0034-4257(90)90085-Z
13. Daughtry, C.S.T., Walthall, C.L., Kim, M.S., Brown de Colstoun, E. and McMurtrey, J.E., 2000. Estimating corn leaf chlorophyll concentration from leaf and canopy reflectance. Remote Sensing Environment, 74 (229 239), 141–152. https://doi.org/10.1016/S0034-4257(00)00113-9
14. David, R. M., Rosser, N. J., & Donoghue, D. N. (2022). Improving above ground biomass estimates of Southern Africa dryland forests by combining Sentinel-1 SAR and Sentinel-2 multispectral imagery. Remote Sensing of Environment, 282, 113232. https://doi.org/10.1016/j.rse.2022.113232

15. Di Giuseppe, F., Benedetti, A., Coughlan, R., Vitolo, C., & Vuckovic, M. (2021). A Global Bottom-Up Approach to Estimate Fuel Consumed by Fires Using Above Ground Biomass Observations. Geophysical Research Letters, 48(21), e2021GL095452. https://doi.org/10.1029/2021GL095452
16. Dogru, A. O., Goksel, C., David, R. M., Tolunay, D., Sözen, S., & Orhon, D. (2020). Detrimental environmental impact of large scale land use through deforestation and deterioration of carbon balance in Istanbul Northern Forest Area. Environmental Earth Sciences, 79, 1-13. https://doi.org/10.1007/s12665-020-08996-3
17. Drusch, M., Del Bello, U., Carlier, S., Colin, O., Fernandez, V., Gascon, F., ... & Bargellini, P. (2012). Sentinel-2: ESA's optical high-resolution mission for GMES operational services. Remote sensing of Environment, 120, 25-36. https://doi.org/10.1016/j.rse.2011.11.026
18. Duncanson, L., Armston, J., Disney, M., Avitabile, V., Barbier, N., Calders, K., ... & Margolis, H. (2021). Aboveground woody biomass product validation good practices protocol.
19. Eggleston, H. S., Buendia, L., Miwa, K., Ngara, T., & Tanabe, K. (2006). 2006 IPCC guidelines for national greenhouse gas inventories. http://www.ipcc-nggip.iges.or.jp/public/2006gl/index.htm
20. Ercanlı, İ., Kurt, A., Şenyurt, M., Günlü, A., Bolat, F. and Keleş, S (2018). Tarsus Yöresi Anadolu Karaçamı Ağaçlarında Hacim Tahminlerinin Yapay Sinir Ağları ile Elde Edilmesi. Anadolu Orman Araştırmaları Dergisi, 4(1), 25-37. http://dergipark.gov.tr/ajfr
21. Fararoda, R., Reddy, R. S., Rajashekar, G., Chand, T. K., Jha, C. S., & Dadhwal, V. K. (2021). Improving forest above ground biomass estimates over Indian forests using multi source data sets with machine learning algorithm. Ecological Informatics, 65, 101392. https://doi.org/10.1016/j.ecoinf.2021.101392
22. Finegan, B., Peña-Claros, M., de Oliveira, A., Ascarrunz, N., Bret-Harte, M. S., Carreño-Rocabado, G., ... & Poorter, L. (2015). Does functional trait diversity predict above-ground biomass and productivity of tropical forests? Testing three alternative hypotheses. Journal of Ecology, 103(1), 191-201. https://doi.org/10.1111/1365-2745.12346
23. Fitzgerald, G., Rodriguez, D. and O'Leary, G. 2010. Measuring and predicting canopy nitrogen nutrition in wheat using a spectral index – the Canopy Chlorophyll Content Index (CCCI). Field Crops Research, 18–324. https://doi.org/10.1016/j.fcr.2010.01.010
24. Foody, G.M. (2003). Remote sensing of tropical forest environments: towards the monitoring of environmental resour-ces for sustainable development. International Journal of Remote Sensing, 24(20): 4035-4046. https://doi.org/10.1080/0143116031000103853
25. Forkuor, G., Dimobe, K., Serme, I., & Tondoh, J. E. (2018). Landsat-8 vs. Sentinel-2: examining the added value of sentinel-2's red-edge bants to land-use and land-cover mapping in Burkina Faso. GIScience & remote sensing, 55(3), 331-354. https://doi.org/10.1080/15481603.2017.1370169
26. Forkuor, G., Zoungrana, J. B. B., Dimobe, K., Ouattara, B., Vadrevu, K. P., & Tondoh, J. E. (2020). Above-ground biomass mapping in West African dryland forest using Sentinel-1 and 2 datasets-A case study. Remote Sensing of Environment, 236, 111496. https://doi.org/10.1016/j.rse.2019.111496
27. Gallaun, H., Zanchi, G., Nabuurs, G. J., Hengeveld, G., Schardt, M., & Verkerk, P. J. (2010). EU-wide maps of growing stock and above-ground biomass in forests based on remote sensing and field measurements. Forest Ecology and Management, 260(3), 252-261. https://doi.org/10.1016/j.foreco.2009.10.011
28. Gitelson, A.A. and Merzlyak, M.N. 1996. Signature analysis of leaf reflectance spectra: algorithm development for remote sensing. Journal of Plant Physiology, 148, 493–500. https://doi.org/10.1016/S0176-1617(96)80284-7
29. Gitelson, A.A., Gritz, U. and Merzlyak, M.N. (2003). Relationships between leaf chlorophyll content and spectral reflec-tance and algorithms for non-destructive chlorophyll assessment in higher plant leaves. Journal of Plant Physio-logy, 160(3), 271-282. https://doi.org/10.1078/0176-1617-00887
30. Gitelson, A.A., Gritz, U. and Merzlyak, M.N. 2003. Relationships between leaf chlorophyll content and spectral reflectance and algorithms for non-destructive chlorophyll assessment in higher plant leaves. Journal of Plant Physiology, 160(3), 271-282. https://doi.org/10.1078/0176-1617-00887
31. Gitelson, A.A., Merzlyak, M.N. and Chivkunova, O.B. 2001. Optical properties and nondestructive estimation of anthocyanin content in plant leaves. Photochemistry and Photobiology, 74(1), 38-45. https://doi.org/10.1562/0031-8655(2001)0740038OPANEO2.0.CO2
32. Gitelson, A.A., Vina, A., Ciganda, V., Rundquist, D.C. and Arkebauer, T.J. 2005. Remote estimation of canopy chlorophyll content in crops. Geophysical Research Letters, 32, L08403. https://doi.org/10.1029/2005GL022688
33. Goel, N.S. and Qin, W. 1994. Influences of canopy architecture on relationships between various vegetation indices and LAI and FPAR: A computer simulation. Remote Sensing Reviews, 10(4), 309-347. https://doi.org/10.1080/02757259409532252
34. Günlü, A.,and Ercanlı, İ. (2020). Artificial neural network models by ALOS PALSAR data for aboveground stand carbon predictions of pure beech stands: a case study from northern of Turkey. Geocarto International, 35(1), 17-28. https://doi.org/10.1080/10106049.2018.1499817

35. Güverçin, İ., and Günlü, A. (2023). Saf Kızılçam (Pinus brutia Ten.) Meşcerelerinde Aktif ve Pasif Uydu Görüntüleri Kullanılarak Topraküstü Biyokütlenin Tahmin Edilmesi (Anamur Orman İşletme Şefliği Örneği). Bartın Orman Fakültesi Dergisi, 25(1), 177-191. https://doi.org/10.24011/barofd.1261299
36. Haboudane, D., Miller, J. R., Pattey, E., Zarco-Tejada, P. J., & Strachan, I. B. (2004). Hyperspectral vegetation indices and novel algorithms for predicting green LAI of crop canopies: Modeling and validation in the context of precision agriculture. Remote sensing of environment, 90(3), 337-352. https://doi.org/10.1016/j.rse.2003.12.013
37. Hardisky, M.A., Klemas, V. and Smart, R.M. (1983). The influence of soil salinity, growth form, and leaf moisture on the spectral radiance of Spartina alterniflora canopies. Photogrammetric Engineering and Remote Sensing, 49: 77 – 83. 0099-1 112/83/4901-77$02.25/0
38. Herold, M., Carter, S., Avitabile, V., Espejo, A. B., Jonckheere, I., Lucas, R., ... & De Sy, V. (2019). The role and need for space-based forest biomass-related measurements in environmental management and policy. Surveys in Geophysics, 40, 757-778. https://doi.org/10.1007/s10712-019-09510-6
39. Hu, T., Zhang, Y., Su, Y., Zheng, Y., Lin, G., & Guo, Q. (2020). Mapping the global mangrove forest aboveground biomass using multisource remote sensing data. Remote sensing, 12(10), 1690. https://doi.org/10.3390/rs12101690
40. Huete, A.R. (1988). A Soil Adjusted Vegetation indices (SAVI). Remote Sensing of Environment, 25:295-309. https://doi.org/10.1016/0034-4257(88)90106-X
41. Hunt Jr, E.R. and Rock, B.N. 1989. Detection of changes in leaf water content using near-and middle-infrared reflectances. Remote sensing of environment, 30(1), 43-54. https://doi.org/10.1016/0034-4257(89)90046-1
42. Jiang, Z.Y., Huete, A.R., Didan, K. and Miura, T. 2008. Development of a two-bant enhanced vegetation indices without a blue bant. Remote Sensing of Environment, 112, 3833–3845. https://doi.org/10.1016/j.rse.2008.06.006
43. Jurgens, C. 1997. The modified normalized difference vegetation indices (mNDVI) a new index to determine frost damages in agriculture based on Landsat TM data. International Journal of Remote Sensing, 18(17), 3583-3594. https://doi.org/10.1080/014311697216810
44. Kaufman, Y.J. and Tanre, D. (1992). Atmospherically resistant vegetation indices (ARVI) for EOS-MODIS. IEEE tran-sactions on Geoscience and Remote Sensing, 30(2): 261-270. 10.1109/36.134076
45. Keleş, S., Günlü, A. and Ercanli, İ. (2021). Estimating aboveground stand carbon by combining Sentinel-1 and Sentinel-2 satellite data: a case study from Turkey. In Forest Resources Resilience and Conflicts pp. 117-126, Elsevier. https://doi.org/10.1016/B978-0-12-822931-6.00008-3
46. Key, C.H. and Benson, N.C. 2006. Landscape assessment (LA). In: Lutes, Duncan C.; Keane, Robert E.; Caratti, John F.; Key, Carl H.; Benson, Nathan C.; Sutherland, Steve; Gangi, Larry J. 2006. FIREMON: Fire effects monitoring and inventory system. Gen. Tech. Rep. RMRS-GTR-164-CD. Fort Collins, CO: US Department of Agriculture, Forest Service, Rocky Mountain Research Station, p. LA-1-55, 164.
47. Kumar, K. K., Nagai, M., Witayangkurn, A., Kritiyutanant, K. and Nakamura, S. (2016). Above ground biomass as-sessment from combined optical and SAR remote sensing data in Surat Thani Province, Thailand. Journal of Geographic Information System, 8(04): 506. 10.4236/jgis.2016.84042
48. Laurin, G. V., Balling, J., Corona, P., Mattioli, W., Papale, D., Puletti, N., ... & Urban, M. (2018). Above-ground biomass prediction by Sentinel-1 multitemporal data in central Italy with integration of ALOS2 and Sentinel-2 data. Journal of Applied Remote Sensing, 12(1), 016008-016008. https://doi.org/10.1117/1.JRS.12.016008
49. Laurin, G. V., Liesenberg, V., Chen, Q., Guerriero, L., Del Frate, F., Bartolini, A., ... & Valentini, R. (2013). Optical and SAR sensor synergies for forest and land cover mapping in a tropical site in West Africa. International Journal of Applied Earth Observation and Geoinformation, 21, 7-16. https://doi.org/10.1016/j.jag.2012.08.002
50. Li, Y., Li, M., Li, C., & Liu, Z. (2020). Forest aboveground biomass estimation using Landsat 8 and Sentinel-1A data with machine learning algorithms. Scientific reports, 10(1), 1-12. https://doi.org/10.1038/s41598-020-67024-3
51. Liu, H.Q. and Huete, A. (1995). A feedback based modification of the NDVI to minimize canopy background and atmospheric noise. IEEE transactions on geoscience and remote sensing, 33(2), 457-465. 10.1109/TGRS.1995.8746027
52. Liu, M., & Popescu, S. (2022). Estimation of biomass burning emissions by integrating ICESat-2, Landsat 8, and Sentinel-1 data. Remote Sensing of Environment, 280, 113172. https://doi.org/10.1016/j.rse.2022.113172
53. Liu, Y., Gong, W., Xing, Y., Hu, X., & Gong, J. (2019). Estimation of the forest stand mean height and aboveground biomass in Northeast China using SAR Sentinel-1B, multispectral Sentinel-2A, and DEM imagery. ISPRS Journal of Photogrammetry and Remote Sensing, 151, 277-289. https://doi.org/10.1016/j.isprsjprs.2019.03.016
54. López-Serrano, P. M., Cárdenas Domínguez, J. L., Corral-Rivas, J. J., Jiménez, E., López-Sánchez, C. A., & Vega-Nieva, D. J. (2019). Modeling of aboveground biomass with Landsat 8 OLI and machine learning in temperate forests. Forests, 11(1), 11. https://doi.org/10.3390/f11010011

55. Louhaichi, M., Borman, M.M. and Johnson, D.E. 2001. Spatially Located Platform and Aerial Photography for Documentation of Grazing Impacts on Wheat. Geocarto International, 16 (1): 65–70. https://doi.org/10.1080/10106040108542184
56. Lu, D. (2005). Aboveground biomass estimation using Landsat TM data in the Brazilian Amazon. International Jour-nal of Remote Sensing, 26(12): 2509-2525. https://doi.org/10.1080/01431160500142145
57. Lucas, R., Accad, A., Randall, L., Bunting, P., & Armston, J. (2008). Assessing human impacts on Australian forests through integration of remote sensing data. Patterns and Processes in Forest Landscapes: Multiple Use and Sustainable Management, 213-239. 10.1007/978-1-4020-8504-8_13
58. Macedo, F. L., Sousa, A. M., Gonçalves, A. C., Marques da Silva, J. R., Mesquita, P. A., & Rodrigues, R. A. (2018). Above-ground biomass estimation for Quercus rotundifolia using vegetation indices derived from high spatial resolution satellite images. European Journal of Remote Sensing, 51(1), 932-944. https://doi.org/10.1080/22797254.2018.1521250
59. Main-Knorn, M., Cohen, W. B., Kennedy, R. E., Grodzki, W., Pflugmacher, D., Griffiths, P., & Hostert, P. (2013). Monitoring coniferous forest biomass change using a Landsat trajectory-based approach. Remote Sensing of Environment, 139, 277-290. https://doi.org/10.1016/j.rse.2013.08.010
60. McFeeters, S.K. 1996. The use of Normalized Difference Water Index (NDWI) in the delineation of open water features, International Journal of Remote Sensing, 17(7):1425–1432. https://doi.org/10.1080/01431169608948714
61. Metternicht, G. 2003. Vegetation Indices derived from high-resolution airborne videogaphy for precision crop management. International Journal of Remote Sensing 24: 2855–2877. https://doi.org/10.1080/01431160210163074
62. NASA (2021). https://www.earthdata.nasa.gov/
63. Navarro, J. A., Algeet, N., Fernández-Landa, A., Esteban, J., Rodríguez-Noriega, P., & Guillén-Climent, M. L. (2019). Integration of UAV, Sentinel-1, and Sentinel-2 data for mangrove plantation aboveground biomass monitoring in Senegal. Remote Sensing, 11(1), 77. https://doi.org/10.3390/rs11010077
64. Nelson, R.F., Kimes, D.S., Salas, W.A. and Routhier, M. (2000). Secondary forest age and tropical forest biomass esti-mation using thematic mapper ımagery: single-year tropical forest age classes, a surrogate for standing biomass, cannot be reliably identified using single-date tm imagery. Bioscience, 50(5): 419-431. https://doi.org/10.1641/0006-3568(2000)050[0419:SFAATF]2.0.CO;2
65. Nguyen, L. V., Tateishi, R., Nguyen, H. T., Sharma, R. C., To, T. T., & Le, S. M. (2016). Estimation of tropical forest structural characteristics using ALOS-2 SAR data. Advances in Remote Sensing, 5(2), 131-144. DOI: 10.4236/ars.2016.52011
66. Nuthammachot, N., Askar, A., Stratoulias, D. and Wicaksono, P. (2022). Combined use of Sentinel-1 and Sentinel-2 data for improving above-ground biomass estimation. Geocarto International, 37(2): 366-376. https://doi.org/10.1080/10106049.2020.1726507
67. Özdemir, G. 2018. Karabük Yöresi Kayın-Göknar Karışık Meşcerelerinde Gövde Çaplarının Yapay Sinir Ağları ile Tahmin Edilmesi, Kastamonu Üniversitesi, Fen Bilimleri Enstitüsü, Orman Mühendisliği Ana Bilimdalı Yüksek Lisans Tezi, 101 s.
68. Perry Jr, C. and Lautenschlager, L.F. 1984. Functional equivalence of spectral vegetation indices. Remote Sensing of Environment, 14(1-3):169-182. https://doi.org/10.1016/0034-4257(84)90013-0
69. Pinty, B. and Verstraete, M.M. 1992. GEMI: A non-linear index to monitor global vegetation from satellites. Vegetatio, vol. 101, pp. 15-20, 1992. https://doi.org/10.1007/BF00031911
70. Poudel, K.P. and Cao, Q.V. 2013. Evaluation of methods to predict Weibull parameters for characterizing diameter distributions. Forest Science, 59(2), 243-252. https://doi.org/10.5849/forsci.12-001
71. Powell, S. L., Cohen, W. B., Healey, S. P., Kennedy, R. E., Moisen, G. G., Pierce, K. B., & Ohmann, J. L. (2010). Quantification of live aboveground forest biomass dynamics with Landsat time-series and field inventory data: A comparison of empirical modeling approaches. Remote Sensing of Environment, 114(5), 1053-1068. https://doi.org/10.1016/j.rse.2009.12.018
72. Puliti, S., Breidenbach, J., Schumacher, J., Hauglin, M., Klingenberg, T. F., & Astrup, R. (2021). Above-ground biomass change estimation using national forest inventory data with Sentinel-2 and Landsat. Remote Sensing of Environment, 265, 112644. https://doi.org/10.1016/j.rse.2021.112644
73. Puliti, S., Hauglin, M., Breidenbach, J., Montesano, P., Neigh, C. S. R., Rahlf, J., ... & Astrup, R. (2020). Modelling above-ground biomass stock over Norway using national forest inventory data with ArcticDEM and Sentinel-2 data. Remote Sensing of Environment, 236, 111501. https://doi.org/10.1016/j.rse.2019.111501
74. Rondeaux, G., Steven, M. and Baret, F. 1996. Optimization of soil-adjusted vegetation indices. Remote Sensing of Environment, 55, 95–107. https://doi.org/10.1016/0034-4257(95)00186-7
75. Rouse, J.W., Hass, R.H., Shell, J.A. and Deering, D.W. (1974). Monitoring vegetation systems in the great plains with ERTS-l. Proceedings, 3rd Earth Resources Technology Satellite Symposium, 1: 309-317.
76. Roy, P.S. and Ravan, S.A. (1996). Biomass estimation using satellite remote sensing data—an investigation on possible approaches for natural forest. Journal of Biosciences, 21(4): 535-561. https://doi.org/10.1007/BF02703218

77. Salum, R. B., Robinson, S. A., & Rogers, K. (2021). A Validated and Accurate Method for Quantifying and Extrapolating Mangrove Above-Ground Biomass Using LiDAR Data. Remote Sensing, 13(14), 2763. https://doi.org/10.3390/rs13142763
78. Santoro, M., Cartus, O., Fransson, J. E., Shvidenko, A., McCallum, I., Hall, R. J., ... & Schmullius, C. (2013). Estimates of forest growing stock volume for sweden, central siberia, and québec using envisat advanced synthetic aperture radar backscatter data. Remote Sensing, 5(9), 4503-4532. https://doi.org/10.3390/rs5094503
79. Santos, J. R., Lacruz, M. P., Araujo, L. S., & Keil, M. (2002). Savanna and tropical rainforest biomass estimation and spatialization using JERS-1 data. International Journal of Remote Sensing, 23(7), 1217-1229. https://doi.org/10.1080/01431160110092867
80. Schroeder, P., Brown, S., Mo, J., Birdsey, R. and Cieszewski, C. (1997). Biomass estimation for temperate broadleaf forests of the United States using inventory data. Forest Science, 43(3): 424-434. https://doi.org/10.1093/forestscience/43.3.424
81. Sibanta, M., Mutanga, O., & Rouget, M. (2016). Discriminating rangeland management practices using simulated hyspIRI, landsat 8 OLI, sentinel 2 MSI, and VENµs spectral data. IEEE Journal of Selected Topics in Applied Earth Observations and Remote Sensing, 9(9), 3957-3969. DOI: 10.1109/JSTARS.2016.2574360
82. Soja, M. J., Quegan, S., d'Alessandro, M. M., Banta, F., Scipal, K., Tebaldini, S., & Ulander, L. M. (2021). Mapping above-ground biomass in tropical forests with ground-cancelled P-bant SAR and limited reference data. Remote Sensing of Environment, 253, 112153.
83. Sripada, R.P. 2005. Determining in-season nitrogen requirements for corn using aerial color-infrared photography.
84. Şahin, A. (2015). Mersin yöresi saf Kızılçam (Pinus brutia Ten.) meşcerelerinde hasılat araştırmaları (Doktora tezi). Erişim adresi: https://tez.yok.gov.tr/UlusalTezMerkezi
85. Thenkabail, P.S., Smith, R.B. and De Pauw, E. 1999. Hyperspectral vegetation indices for determining agricultural crop characteristics. CEO research publication series No. 1. Center for Earth Observation, Yale University Press, New Haven.
86. Tiwari, A.K. (1994). Mapping forest biomass through digital processing of IRS-IA data. International Journal of Remo-te Sensing, 15(9): 1849-1866. https://doi.org/10.1080/01431169408954212
87. Tomppo, E., Nilsson, M., Rosengren, M., Aalto, P. and Kennedy, P. (2002). Simultaneous use of Landsat-TM and IRS-1C WiFS data in estimating large area tree stem volume and aboveground biomass. Remote Sensing of Envi-ronment, 82(1): 156-171. https://doi.org/10.1016/S0034-4257(02)00031-7
88. Torres, R., Snoeij, P., Geudtner, D., Bibby, D., Davidson, M., Attema, E., ... & Rostan, F. (2012). GMES Sentinel-1 mission. Remote sensing of environment, 120, 9-24. https://doi.org/10.1016/j.rse.2011.05.028
89. Tucker, C.J. (1980). A spectral method for determining the percentage of green herbage material in clipped sample. Remote Sensing of Environment, 9(2): 175–181. https://doi.org/10.1016/0034-4257(80)90007-3
90. Turgut, R., & Günlü, A. (2022). Estimating aboveground biomass using Landsat 8 OLI satellite image in pure Crimean pine (Pinus nigra JF Arnold subsp. pallasiana (Lamb.) Holmboe) stands: a case from Turkey. Geocarto International, 37(3), 720-734. https://doi.org/10.1080/10106049.2020.1737971
91. Vafaei, S., Soosani, J., Adeli, K., Fadaei, H., Naghavi, H., Pham, T. D., & Tien Bui, D. (2018). Improving accuracy estimation of Forest Aboveground Biomass based on incorporation of ALOS-2 PALSAR-2 and Sentinel-2A imagery and machine learning: A case study of the Hyrcanian forest area (Iran). Remote Sensing, 10(2), 172. https://doi.org/10.3390/rs10020172
92. Vaglio Laurin, G., Del Frate, F., Pasolli, L., Notarnicola, C., Guerriero, L., & Valentini, R. (2013). Discrimination of vegetation types in alpine sites with ALOS PALSAR-, RADARSAT-2-, and lidar-derived information. International journal of remote sensing, 34(19), 6898-6913. https://doi.org/10.1080/01431161.2013.810823
93. Vincini, M., Frazzi, E. and D'Alessio, P. (2007). Comparison of narrow-bant and broad-bant vegetation indexes for canopy chlorophyll density estimation in sugar beet. In J. V. Stafford (Ed.), Precision agriculture '07: Proceedings of the 6th European Conference on Precision Agriculture (pp. 189–196). Wageningen, The Netherlands: Wageningen Academic Publishers.
94. Wang, F., Huang, J., Tang, Y. and Wang, X. 2007. New vegetation indices and its application in estimating leaf area index of rice. Rice Science, 14:195-203. https://doi.org/10.1016/S1672-6308(07)60027-4
95. Zhao, P., Lu, D., Wang, G., Liu, L., Li, D., Zhu, J., & Yu, S. (2016). Forest aboveground biomass estimation in Zhejiang Province using the integration of Landsat TM and ALOS PALSAR data. International Journal of Applied Earth Observation and Geoinformation, 53, 1-15. https://doi.org/10.1016/j.jag.2016.08.007
96. Zheng, D., Rademacher, J., Chen, J., Crow, T., Bresee, M., Le Moine, J. and Ryu, S.R. (2004). Estimating aboveground biomass using Landsat 7 ETM+ data across a managed landscape in northern Wisconsin, USA. Remote Sensing of Environment, 93(3): 402-411. https://doi.org/10.1016/j.rse.2004.08.008
97. Zhu, Y., Liu, K., Liu, L., Wang, S., & Liu, H. (2015). Retrieval of mangrove aboveground biomass at the individual species level with worldview-2 images. Remote Sensing, 7(9), 12192-12214. https://doi.org/10.3390/rs70912192

Figures

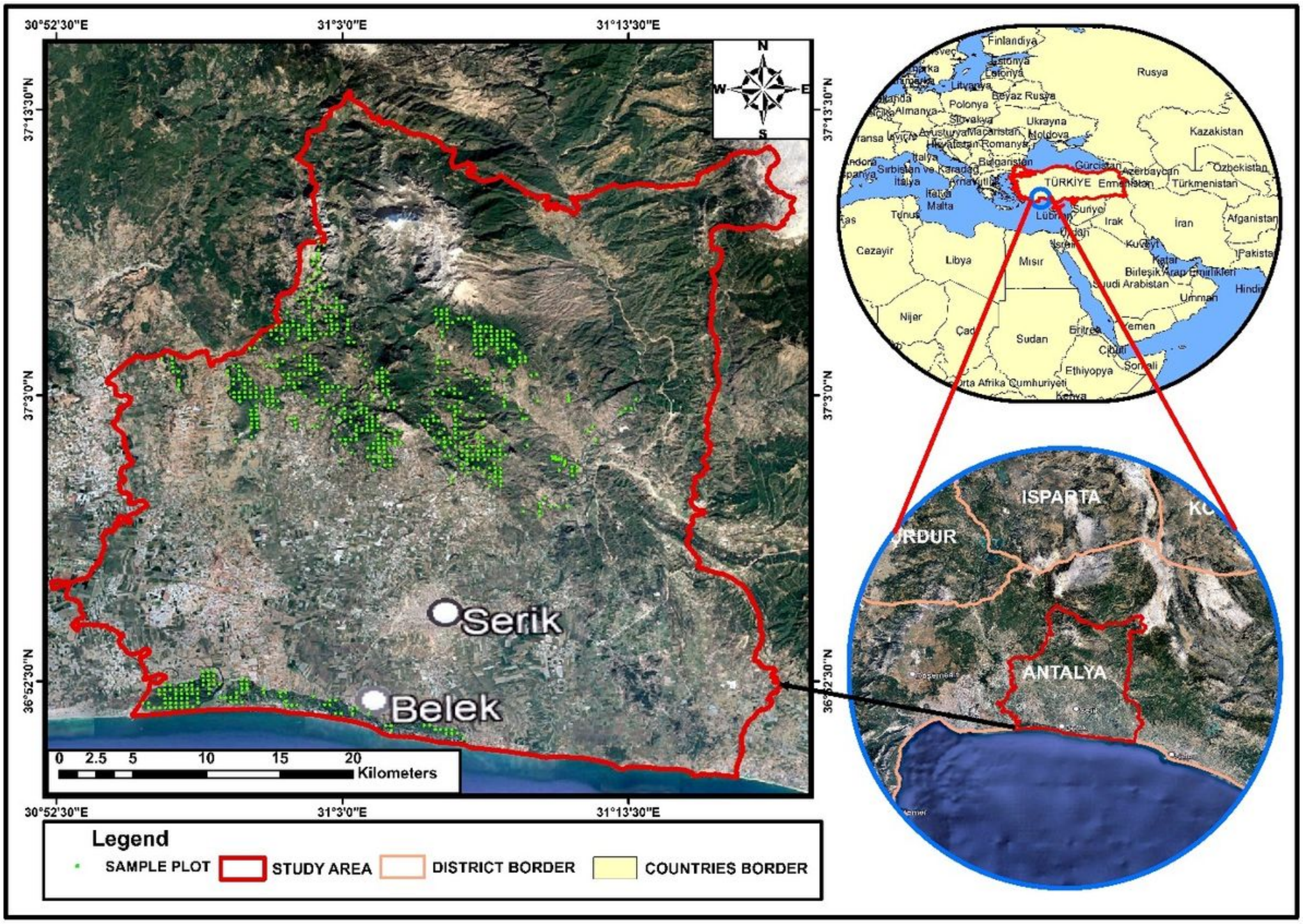

Figure 1

Location of the study area

In the study, forest management inventories s of the diameter data at breast height ($d_{1.3}$) of trees 8 cm and above in 224 sample plots, which were systematically determined at 300 x 300m spacing distance for pure Calabrian pine stands, were used. Sentinel-2 satellite image for 26.05.2021 – 24.08.2021 and 22.11.2021, Sentinel-1A satellite image dated 26.11.2021, and ALOS-PALSAR image for digital elevation model, regarding the year of the measurements were obtained. The properties of Sentinel-2 and Sentinel-1A satellite images are shown in Table 1 and Table 2 (Nasa 2021).

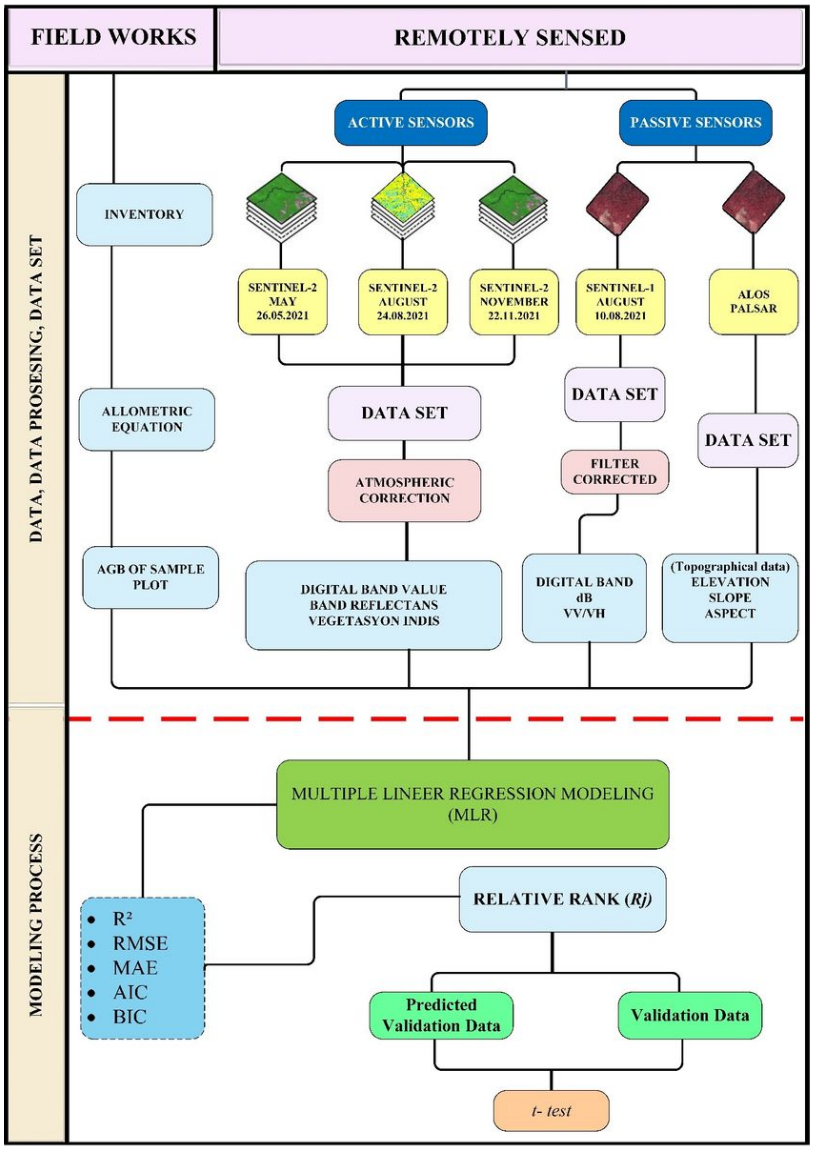

Figure 2

Overall methodology of the study.

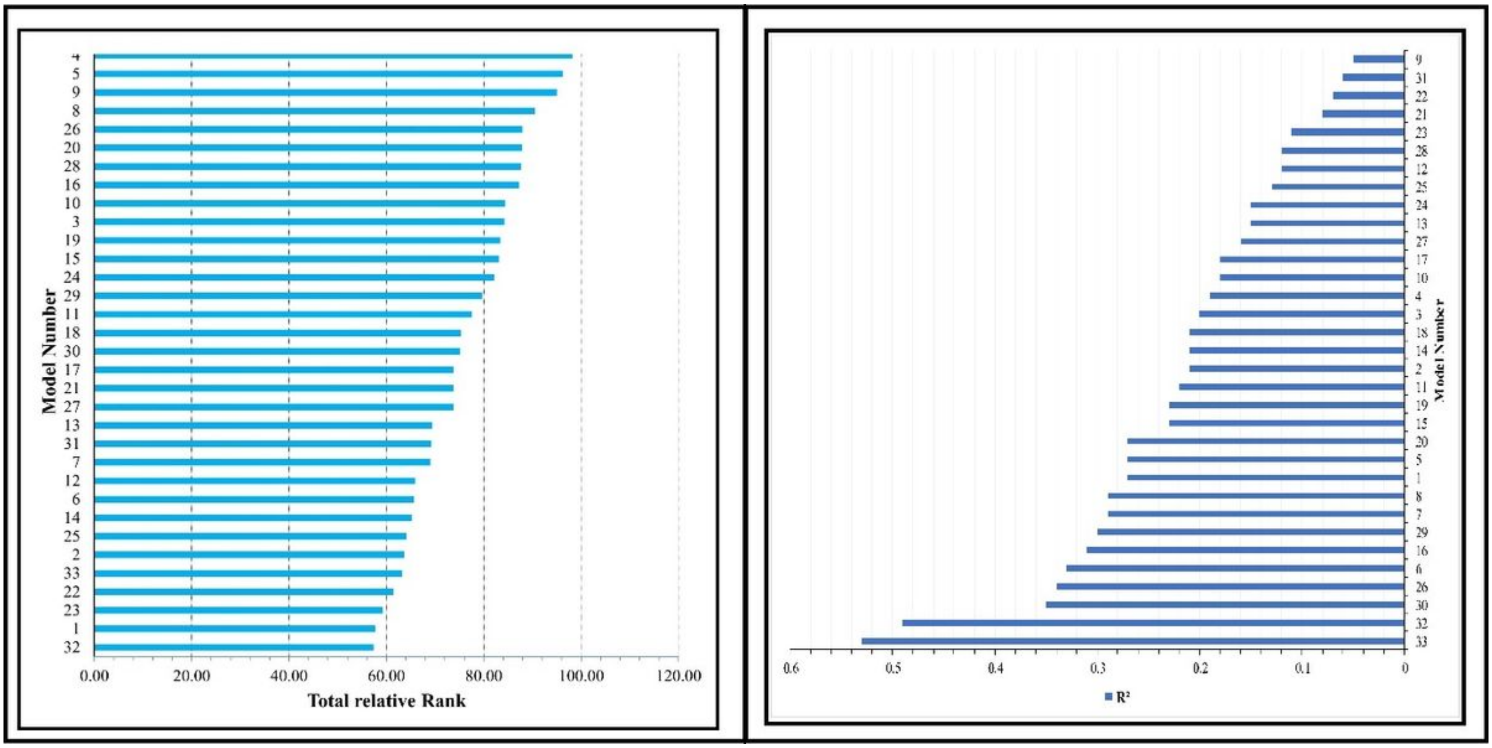

Figure 3

Success levels of regression models

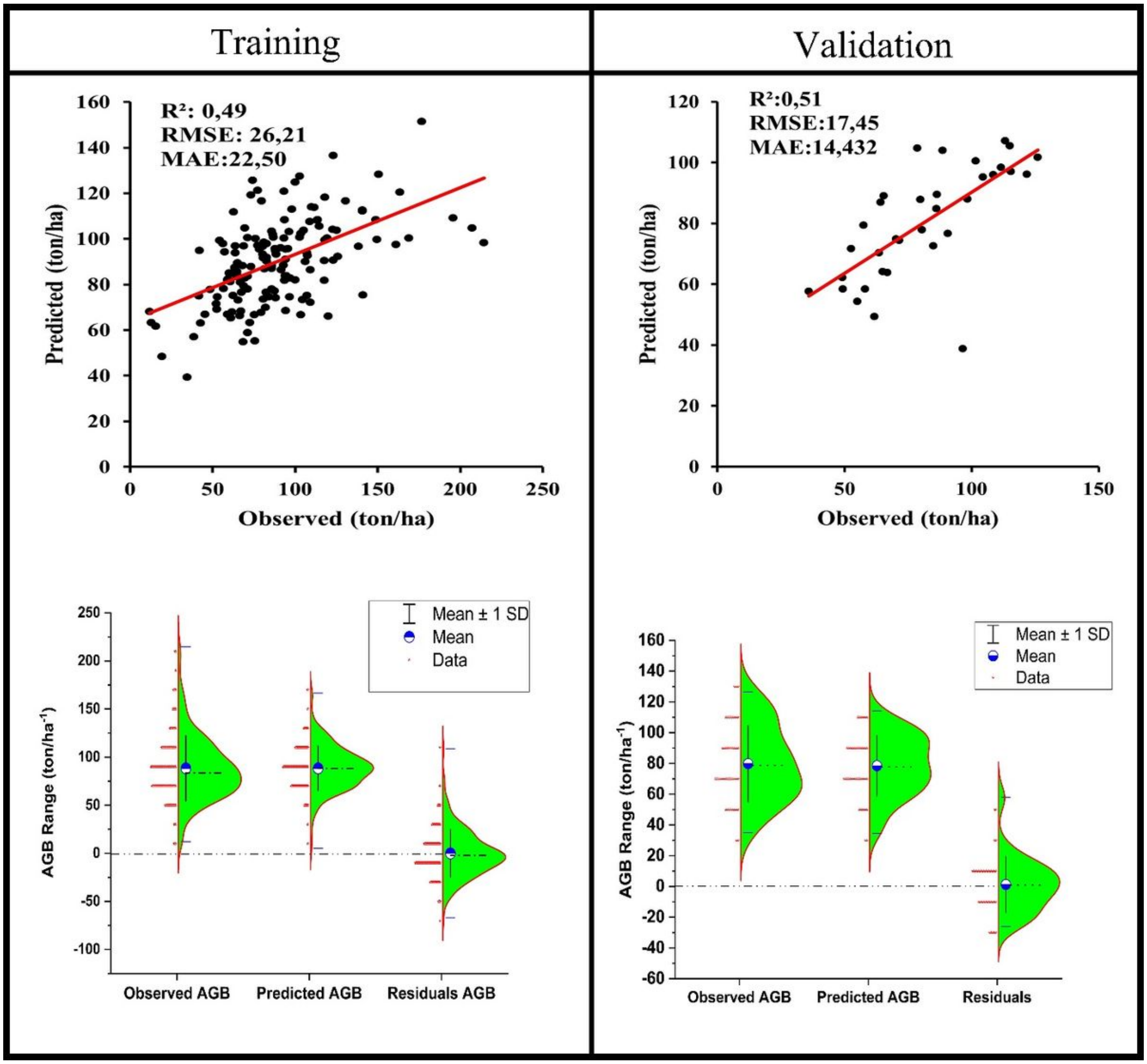

Figure 4

Predicted and observed AGB plots for independent variables and their combinations

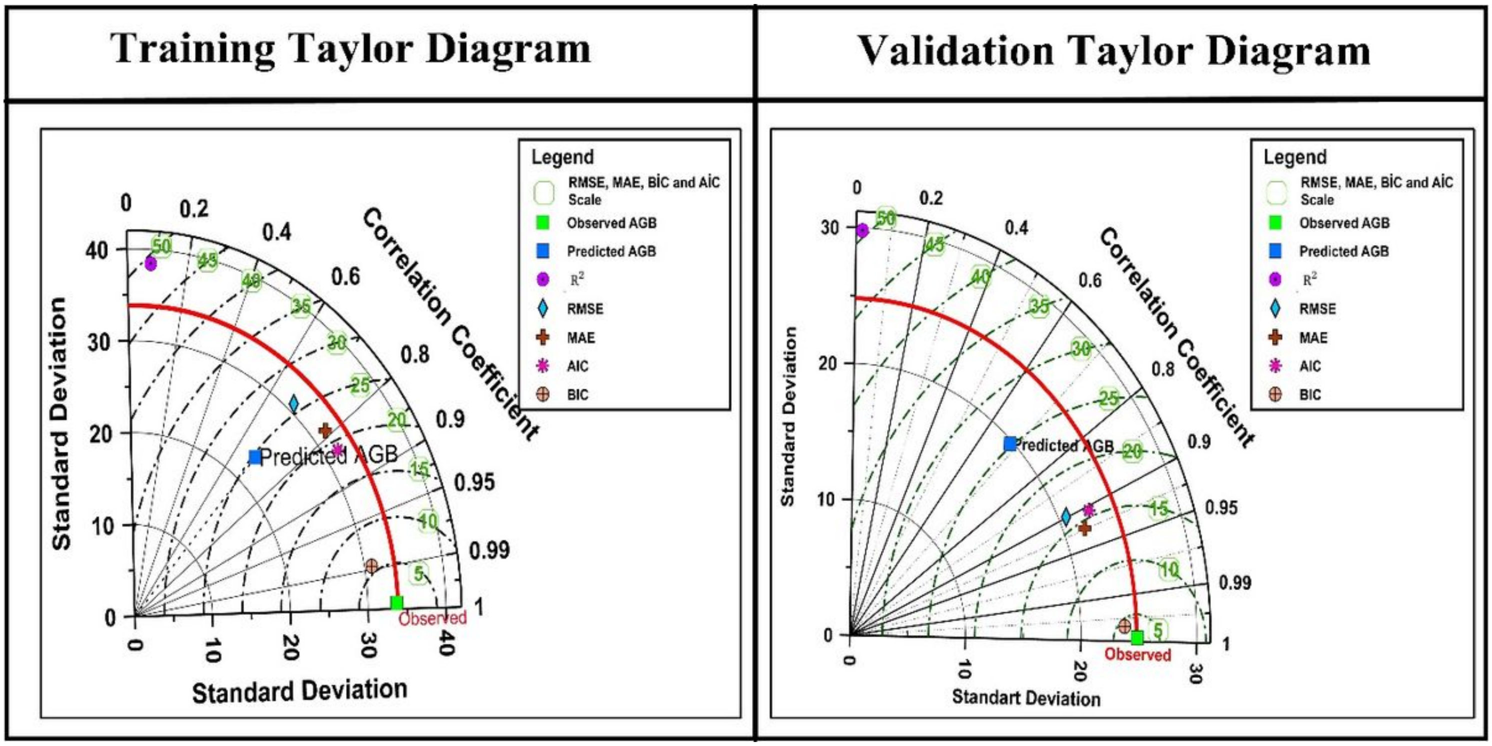

Figure 5

Taylor diagrams of training and validation